JGR Atmospheres

RESEARCH ARTICLE
10.1029/2018JD028862

A New Regional Climate Model for POLAR-CORDEX: Evaluation of a 30-Year Hindcast with COSMO-CLM^2 Over Antarctica

N. Souverijns[1], A. Gossart[1], M. Demuzere[2], J. T. M. Lenaerts[3], B. Medley[4], I. V. Gorodetskaya[5], S. Vanden Broucke[1], and N. P. M. van Lipzig[1]

[1]Department of Earth and Environmental Sciences, KU Leuven, Leuven, Belgium, [2]Department of Environment, Ghent University, Ghent, Belgium, [3]Department of Atmospheric and Oceanic Sciences, University of Colorado Boulder, Boulder, CO, USA, [4]Cryospheric Sciences Laboratory, NASA Goddard Space Flight Center, Greenbelt, MD, USA, [5]Centre for Environmental and Marine Sciences, Department of Physics, University of Aveiro, Aveiro, Portugal

Key Points:
- A long-term integration with the COSMO-CLM2 Regional Climate Model for the Antarctic is presented
- Climate representation performance is comparable to state-of-the-art models
- The simulation is a contribution to CORDEX over Antarctica (POLAR-CORDEX) and CORDEX-CORE

Supporting Information:
- Supporting Information S1

Correspondence to:
N. Souverijns,
niels.souverijns@kuleuven.be

Citation:
Souverijns, N., Gossart, A., Demuzere, M., Lenaerts, J. T. M., Medley, B., Gorodetskaya, I. V., et al. (2019). A new regional climate model for POLAR-CORDEX: Evaluation of a 30-year hindcast with COSMO-CLM^2 over Antarctica. *Journal of Geophysical Research: Atmospheres*, *124*, 1405–1427. https://doi.org/10.1029/2018JD028862

Received 24 APR 2018
Accepted 20 JAN 2019
Accepted article online 25 JAN 2019
Published online 8 FEB 2019

Abstract Continent-wide climate information over the Antarctic Ice Sheet (AIS) is important to obtain accurate information of present climate and reduce uncertainties of the ice sheet mass balance response and resulting global sea level rise to future climate change. In this study, the COSMO-CLM^2 Regional Climate Model is applied over the AIS and adapted for the specific meteorological and climatological conditions of the region. A 30-year hindcast was performed and evaluated against observational records consisting of long-term ground-based meteorological observations, automatic weather stations, radiosoundings, satellite records, stake measurements and ice cores. Reasonable agreement regarding the surface and upper-air climate is achieved by the COSMO-CLM^2 model, comparable to the performance of other state-of-the-art climate models over the AIS. Meteorological variability of the surface climate is adequately simulated, and biases in the radiation and surface mass balance are small. The presented model therefore contributes as a new member to the COordinated Regional Downscaling EXperiment project over the AIS (POLAR-CORDEX) and the CORDEX-CORE initiative.

1. Introduction

Detailed and adequate climate information over the Antarctic Ice Sheet (AIS) is considered of very large importance by several global climate research initiatives, such as the international COordinated Regional Downscaling EXperiment (CORDEX) project (Giorgi et al., 2009), CORDEX-CORE (Giorgi & Gutowski, 2016; Gutowski et al., 2016), POLAR-CORDEX initiatives (Koenigk et al., 2015; Scinocca et al., 2016), and the Intergovernmental Panel on Climate Change fifth assessment report (Stocker et al., 2013). Jones et al. (2016) stress the need for an increase in the number of long-term simulations of different regional climate models (RCMs) over the AIS in order to obtain an ensemble representation of the present and the future Antarctic climate. As such, a better understanding of the surface mass balance (SMB) and its impact on sea level is achieved. In order to facilitate near-future developments of high-resolution RCM simulations, nonhydrostatic models are preferred (Giorgi & Gutowski, 2015, 2016).

RCMs are an important and valuable tool for improving our understanding of the climate of different regions in the world. They simulate atmospheric processes and incorporate interactions with the surface from the regional to local scale and bring a large added value compared to global climate models (GCMs; Feser et al., 2011; Rummukainen, 2016). For remote locations such as the AIS, where the spatial and temporal extent of the observational network is limited, RCMs are indispensable as they provide climatological information covering the full continent at relatively high resolution (van Wessem, Reijmer, Lenaerts, et al., 2014). For example, output of multimodel RCM studies can be used to get accurate estimates of historical and projected future changes in the SMB of the AIS, which has a direct impact on sea level rise and therefore on coastal areas around the world (Agosta et al., 2013; Favier et al., 2017; Lenaerts et al., 2012; Lenaerts et al., 2016).

RCM simulations over the AIS are nevertheless few in number and limited to a few distinct models, namely, the Modèle Atmosphérique Regional (MAR; Gallée & Schayes, 1994), the Antarctic Mesoscale Prediction System (AMPS; POLAR-WRF; Bromwich et al., 2013; Parish & Bromwich, 2007), and the Regional

Atmospheric Climate Model (RACMO2; van de Berg et al., 2005). From these models, only POLAR-WRF is nonhydrostatic. These models are adapted to specific polar climate characteristics in order to constrain distinct variables over the ice sheet, such as the SMB (Gallée et al., 2011; Lenaerts et al., 2012; Ligtenberg et al., 2013; van Lipzig et al., 2002; van Wessem, Reijmer, Morlighem, et al., 2014), drifting snow (Gallée et al., 2013; Lenaerts & van den Broeke, 2012), the surface energy balance (Kuipers Munneke et al., 2011; van Lipzig et al., 1999; van Wessem, Reijmer, Lenaerts, et al., 2014), cloud and precipitation radiative properties (Gallée & Gorodetskaya, 2010), or other basic climate variables, for example, temperature and wind speed (Dethloff et al., 2010; Sanz Rodrigo et al., 2013; van den Broeke & van Lipzig, 2003; Xin et al., 2014). As only a limited number of long-term simulations are available, future projections of the AIS climate are still mainly deduced from GCMs. These GCMs do not appropriately resolve mesoscale variability and are not fully adapted for specific Antarctic conditions. Furthermore, the spatial resolution of GCMs, usually exceeding 100 km, is too coarse to adequately capture typical Antarctic climatic features, such as katabatic winds and blowing snow.

The regional-scale COnsortium for Small-scale MOdeling (COSMO) model (Rockel et al., 2008) is an RCM which has been applied over several regions of the world at different spatial and temporal resolutions. Its operation over the AIS is mainly limited to a few simulations in numerical weather prediction mode, studying individual snowfall events (Wacker et al., 2009) or polynya occurrence (Ebner et al., 2014; Haid et al., 2014). Some simulations with COSMO have been executed over polar regions (Gutjahr et al., 2016; Zhou et al., 2014), but these are mainly restricted to very short periods or studies of specific atmospheric phenomena.

Previous studies have proven the capability of the COSMO model to study short-term atmospheric processes in polar regions. Furthermore, the COSMO model is a nonhydrostatic model, complying with the requirements of future RCMs (Giorgi & Gutowski, 2015, 2016). As such, it is timely to apply the model for long-term simulations, addressing the requirements of the POLAR-CORDEX initiative to attain a multimodel ensemble of RCM studies over the AIS. This is facilitated by coupling the model to the Community Land Model (Oleson & Lawrence, 2013), which has recently been adapted for Antarctic climate conditions (van Kampenhout et al., 2017). This improved land model allows for a state-of-the-art representation of the snow pack and interactions between the surface and the atmosphere. The coupled version is referred to as COSMO-CLM^2 (Davin et al., 2011).

In this study, the COSMO-CLM^2 model is applied over the AIS, while introducing some modifications to the atmospheric component, the land-surface model, and the interactions between the two. In order to assess the performance of the model in simulating the Antarctic climate, an evaluation of both the near-surface and upper air climate is performed. In this respect, a high-quality, long-term database of meteorological observations is compiled from publicly available sources, including information of temperature, wind speed, relative humidity, albedo, SMB, and surface radiation for several locations on the AIS. The results of the 30-year hindcast model simulation are compared to this database, resulting in an extensive and broad evaluation.

2. Model Description and Data

2.1. Model Setup

The COSMO model (version 5.0) is a nonhydrostatic RCM developed by the German Weather Service and the scientific community (Rockel et al., 2008; Wouters et al., 2016). In this work, COSMO-CLM^2 is applied over a spatial domain covering the whole AIS. The model dynamically downscales boundary conditions from a global driving model with a coarse resolution to the regional fine-scale model grid. The boundary conditions for the long-term simulation are the European Centre for Medium-Range Weather Forecasts Interim Re-Analysis (ERA-Interim; Dee et al., 2011). ERA-Interim is generally considered the best reanalysis product over the AIS (Bracegirdle & Marshall, 2012) and is available from 1979 to 2017 at a spatial resolution of 0.7°. Upper-air relaxation using spectral nudging was applied to the top layers of the atmosphere following the approach of van de Berg and Medley (2016), that is, adjusting temperature and wind speed at the upper model levels to the large-scale driving model, ERA-Interim. Relaxation toward ERA-Interim is strongest near the top of the atmosphere, declining sharply toward the surface (<10% at 600 hPa in case the surface is at 1,000 hPa; van de Berg & Medley, 2016). The COSMO-CLM^2 simulation has a horizontal resolution of 0.22° (about 25 km) and 40 vertical levels in the atmosphere derived from the height based Gal-Chen coordinate. The uppermost layer is located at 20 hPa, and 10 levels are located below 1,000 m above ground level (a.g.l.), with the lowest three levels situated at 20, 50, and 90 m a.g.l. The model has a time step of 120 s

and the simulation spans the time window 1983–2016. The first four years of the simulation are discarded in order to assure the spin-up of the snow pack, so we focus our analysis on the period 1987–2016.

2.2. Model Adjustments

The COSMO model was originally developed for applications over the European continent. Although it has been used in many regions of the world, simulations over polar regions are limited. When applying an RCM over those areas, adaptations are needed in order to better represent the specific conditions over the AIS (Cassano et al., 2001; King et al., 2001; Reijmer et al., 2005; van Lipzig et al., 1999). The adjustments that were made to COSMO prior to the application of the model for the 30-year hindcast simulation are described below.

The COSMO model is coupled to the Community Land Model version 4.5 (Oleson & Lawrence, 2013), using the OASIS3-MCT coupler (Will et al., 2017). This coupled model is referred to as COSMO-CLM^2 and is described in Davin et al. (2011). In this coupled model, the snowpack consists of five different layers for which hydrology, compaction, and heat exchange are calculated individually (Oleson & Lawrence, 2013). Adaptations to the representation of perennial snow in the Community Land Model have been implemented as proposed by van Kampenhout et al. (2017) in order to better represent the snow surface and mass balance of ice sheets and glaciers. These encompass a new implementation of the fresh snow density parametrization (Liston et al., 2007), reducing excessive melt rates over the AIS (Lenaerts et al., 2016), fixing a bug in the snow capping (van Kampenhout et al., 2017), and accounting for the compaction effect of drifting snow in a parametrized way (Vionnet et al., 2012). The snow pack depth has been kept constant at 1-m snow water equivalent in order to reduce spin-up time and since interactions with the atmosphere are mainly limited to the top few meters (van Kampenhout et al., 2017). As such, a state-of-the-art representation of the surface of the AIS is achieved.

The roughness length of snow has been set to recommended values by Nishimura et al. (2014) and Smeets and van den Broeke (2008), who found that at the equilibrium line of glaciers in summer, the smooth surface leads to snow roughness lengths in the order of 10^{-5} m for the Greenland Ice Sheet. Although this value might be too low for the interior of the continent, it gives a correct representation of the katabatic wind at the coastal margins of the AIS and the ice shelves.

The near-surface atmosphere over the AIS is typically characterized by a temperature inversion in austral winter (June-July-August), where cold and dense air is overlaid by warmer air. This indicates a stable boundary layer and limits convection (Genthon et al., 2013; Handorf et al., 1999; King et al., 2006). Unstable conditions occur rarely over the AIS and are only observed during austral summer season (December-January-February) over the coastal areas. For the inland areas, near-neutral conditions can occur during this season (van As et al., 2006; Pietroni et al., 2014). Turbulence in the COSMO-CLM^2 model is calculated using a turbulent kinetic energy scheme. In order to represent strong stable conditions typical for the AIS, the minimum turbulent diffusion coefficients and the thermal circulation term in this scheme need to be reduced compared to the standard settings (Buzzi et al., 2011; Hebbinghaus & Heinemann, 2006). Following Cerenzia et al. (2014), the minimum turbulent diffusion coefficients have been set to 0.03 m^2/s, while the thermal circulation term equals 10, achieving an adequate representation of the boundary layer structure.This representation of the boundary layer is used to diagnose meteorological information below the lowest model level, such as 2-m temperature and 10-m wind speed, during the model integration. It must be noted that the lowest model level, located at 20 m, is deficient in representing inversions that have their maximum in temperature at lower heights, leading to potential erroneous representation of diagnostically derived variables close to the surface, such as 2-m temperature and 10-m wind speed.

The SMB is one of the key components of the AIS climate and directly affects global sea level (Martin-Español et al., 2017). It is constructed of several terms: precipitation, erosion or deposition of snow by wind, melt water runoff, surface sublimation, and blowing snow sublimation (van den Broeke et al., 2004). As snowfall is by far the largest positive contributor to the AIS integrated SMB, it is important to realistically simulate it in COSMO-CLM^2. Thus, representing this value in the model is of very high importance for historical and future climate simulations and their predictions of sea level rise. Adjustments were made to the two-moment cloud microphysics parametrization scheme (Seifert & Beheng, 2006) to better account for the limited availability of aerosols that can act as cloud and ice condensation nuclei (CCN and IN, respectively). The two-moment scheme parametrizes all relevant homogeneous and heterogeneous nucleation processes including the activation of CCN and IN. Four frozen hydrometeor classes are considered: ice, snow, graupel,

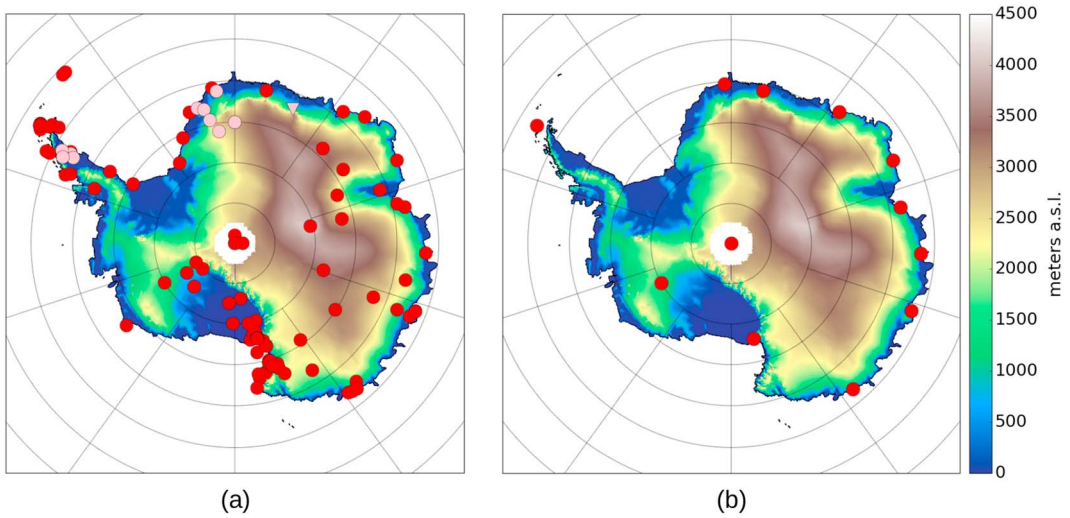

Figure 1. Observational network with data availability of minimal 10 years for (a) ground-based observations and (b) radiosoundings. Pink indicates the availability of measurements of relative humidity and radiative fluxes by automatic weather stations. Background elevation data are obtained from the Radarsat Antarctic Mapping Project Digital Elevation Model (Liu et al., 2015).

and hail, while cloud nucleation rates are defined based on aerosol concentrations. Over the AIS, the number of observed CCN and IN is limited, but highly variable depending on location/distance from the coast (Chaubey et al., 2011; Herenz et al., 2019; Kyrö et al., 2013). For IN, we reduced the number of soot and organic particles of Phillips et al. (2008) to 10% of its original value. CCN concentrations are obtained from the maritime simulations of Khain et al. (2004), which are indicative for pristine regions. Furthermore, in order to limit a rapid conversion of ice to snow, the ice particle distribution is modified following Paukert and Hoose (2014), while the deposition coefficient is set to 0.05 (Gierens, 2003; Köhler & Seifert, 2015).

2.3. Observations

Meteorological observations over the AIS are scarce and limited to a few distinct locations, which usually colocate with scientific research stations. Furthermore, long-term time series are usually limited to the basic near-surface meteorological variables, such as temperature and wind speed (Sanz Rodrigo et al., 2013). Observations are retrieved from the SCAR database (Turner et al., 2004), the AMRC program (http://amrc.ssec.wisc.edu/), the Australian Antarctic AWS data set (http://aws.acecrc.org.au/) and the Italian Antarctic Research Program (http://www.climantartide.it). From this record, in total 101 individual sites were retained, having monthly temperature and wind speed observations for a time period of at least 10 years (Figure 1). More than 50% of the locations have observations available for periods exceeding 20 years. An overview of all ground-based wind and temperature observations including their temporal availability is presented in Table S3 in the supporting information. Wind speed is generally not measured at the same height for each location. All wind speed observations are extrapolated to 10 m a.g.l. assuming a Monin-Obukov logarithmic vertical profile at neutral conditions (Sanz Rodrigo, 2011). Temperature measurements are generally achieved for all stations at 2–3 m a.g.l. In the last decade, automatic weather stations (AWSs) have been installed on several remote locations over the AIS. These devices do not only record temperature and wind speed but also radiative fluxes and relative humidity. Relative humidity measurements are recorded with respect to water and are converted to humidity with respect to ice using the conversion of Anderson (1994). Long-term information of these variables are available for 11 AWSs over the AIS, which are part of the IMAU Antarctic AWS Project (https://www.projects.science.uu.nl/iceclimate/aws/antarctica.php, Table S4 in the supporting information). These observations are nevertheless mainly located in Dronning Maud Land and the ice shelves of the Antarctic Peninsula (Figure 1).

Several scientific stations across the AIS launch radiosondes each day at 12-hourly intervals (00 and 12 UTC). Monthly average temperature, wind speed, and humidity profiles are retrieved from the Integrated Global Radiosonde Archive Version 2, a collection of radiosounding data across several sources (Durre et al., 2018). A total of 12 locations have observations for a time period longer than 10 years (Figure 1). Most of these stations are located on coastal sites (9), while only two are located inland and one is situated on the Antarctic

Peninsula. A detailed overview of these observations, including their temporal availability, can be found in the supporting information (Table S5).

Near-surface and upper air climatology is evaluated by comparing each individual observational location with the mean of all grid boxes of which the center is located within 50 km of the measurement site. For all observations, an average seasonal comparison is visualized. Apart from this, the mean absolute error (MAE) and Pearson correlation coefficient is calculated. The MAE is defined as the average of the differences between each monthly observed and modeled meteorological value. The Pearson correlation coefficient also takes into account each individual monthly observation. As such, apart from the average performance, also the quality of the temporal variability simulated by the model is assessed. Lastly, for a selection of stations on the coast, inland and the Antarctic Peninsula, the temporal and interannual variability is visualized.

Apart from meteorological observations of ground-based measurements and radiosoundings, satellite products can also be used to retrieve relevant climatological information over the AIS. The MODerate-resolution Imaging Spectroradiometer (MODIS) sensor on board of the Terra and Aqua satellites observe the albedo of the underlying surface in cloud-free conditions (Schaaf et al., 2002). The 16-day albedo product was shown to correctly represent the albedo of the Greenland Ice Sheet compared to in situ measurements (Stroeve et al., 2005). MODIS provides two albedo products: black-sky (directional hemispherical) and white-sky (bihemispherical) albedo. The actual albedo is a linear combination of both quantities. For the AIS however, both measures are similar during austral summer, apart from the locations closest to the poles (Stroeve et al., 2005). In this study, only the white-sky albedo is used. A comparison between the black-sky and white-sky albedo climatology is performed showing minor differences between both (Figure S1 in the supporting information). To facilitate the comparison, the MODIS albedo product was aggregated to the COSMO-CLM^2 grid.

Moreover, a compilation of quality-controlled SMB data from various sources gathered by Favier et al. (2013) was used in this study. SMB measurement methods vary from stake measurements and ice cores to rain gauges or ground penetrating radar, leading to a database consisting of 1,432 single-year observations. In addition to the quality check performed by Favier et al. (2013), data with a height discrepancy higher than 150 m between the elevation given in the database and the mean height of the corresponding COSMO-CLM^2 pixel are also discarded, leading to a total of 1,094 observations. Furthermore, 576 ice core data points originating from the Thomas et al. (2017) database were used in this analysis.

The SMB consists of several components: precipitation, erosion or deposition, melt water runoff, surface sublimation, and blowing snow sublimation (van den Broeke et al., 2004). The balance between these components determines the amount of net accumulation or ablation at the local scale. In the COSMO-CLM^2 model, we obtain a simplified modeled SMB by subtracting the sublimation from the precipitation field. Other processes such as blowing snow erosion and sublimation are not represented and therefore not taken into account in the modeled SMB. The COSMO-CLM^2 simulated 1987–2016 annual mean SMB is compared with the observational data set of Favier et al. (2013) and Medley and Thomas (2019). The 1,670 single-year observation points are compared to the SMB value of the corresponding COSMO-CLM^2 grid cell of the same year. We use here the mean value of each pixel; no interpolation or weighing method has been applied to account for the distance of the observation point to the center of the grid mesh. Each of the single-year observation is considered independently, and observations within the same pixel are individually compared to the mean corresponding COSMO-CLM^2 SMB value. Then, a classification of the SMB according to elevation is performed: We bin the observations and model results in five classes, according to elevation and roughly corresponding to different zones of the AIS: less than 500 m a.g.l.: the ice shelves, from 500 to 1,000 m a.g.l. to represent the coastal area, 1,000 to 2,000 m a.g.l., corresponding roughly to the escarpment zone, and lastly the interior of Antarctica: 2000 to 3,000 m a.g.l. and higher than 3,000 m a.g.l.

Lastly, a continent-wide SMB reconstruction is available based on ice cores for the 1987–2010 time period: Medley and Thomas (2019) use the temporal SMB information from ice cores, with the spatial information from reanalysis products. This method is adapted from Monaghan et al. (2006) and uses meteorological reanalysis data fields to reconstruct the atmospheric circulation and the topography-wind relation in order to define zones of influence and of coherent snowfall that correlate to the individual observations in that area at annual time scales.

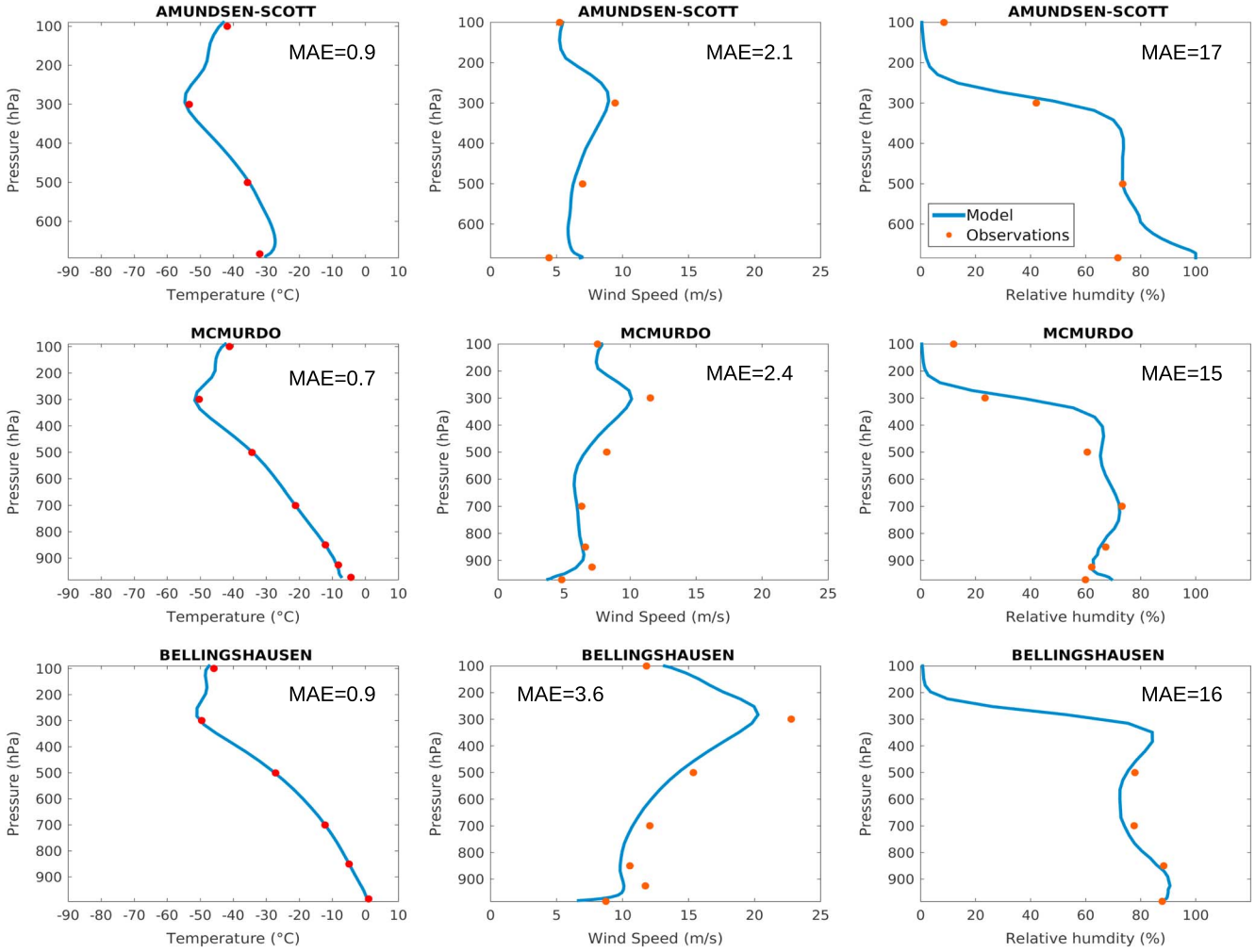

Figure 2. Average radiosounding profiles and vertical model profiles for the austral summer season (December-January-February) of temperature (first column), wind speed (second column), and relative humidity (third column). Three stations are displayed: Amundsen Scott (inland), McMurdo (coastal), and Bellingshausen (Antarctic Peninsula). The blue line denotes the average field in the model, while the red dots indicate radiosounding average values. The top of the profile is always located at the 100-hPa level, while the lower boundary equals the average surface pressure. MAE denotes the mean absolute error calculated based on each individual monthly observation and does not include the surface and the 100-hPa level.

Finally, surface mass changes of the AIS from the satellite gravimetry mission GRACE (Gravity Recovery and Climate Experiment; Tapley et al., 2004) are used, more specifically the Gravimetric Mass Balance gridded product by TU Dresden (Groh & Horwath, 2016). A direct comparison of mass anomaly retrieved from the altimetry data to COSMO-CLM^2 output is not possible, as the other SMB components also impacts AIS mass changes. However, subsampling the ice sheet into drainage basins (Zwally et al., 2012) enables to select smaller areas, such as Dronning Maud Land. For this region, two episodes of large snowfall anomalies were observed in 2009 and 2011 (Gorodetskaya et al., 2013; Gorodetskaya et al., 2014). Since the other components of the SMB (erosion or deposition of snow, melt water runoff, surface sublimation, and blowing snow sublimation) exhibited little changes during this period (Lenaerts et al., 2012; Rignot et al., 2011), these anomalies in SMB can be attributed to the large snowfall events (Boening et al., 2012; Shepherd et al., 2012).

The compilation of this quality-controlled database consisting of ground-based and upper air meteorology, surface energy balance, albedo, and SMB observations from several publicly available sources is unprecedented over the AIS. Hence, it is of major importance regarding the evaluation and development of climate models over the region.

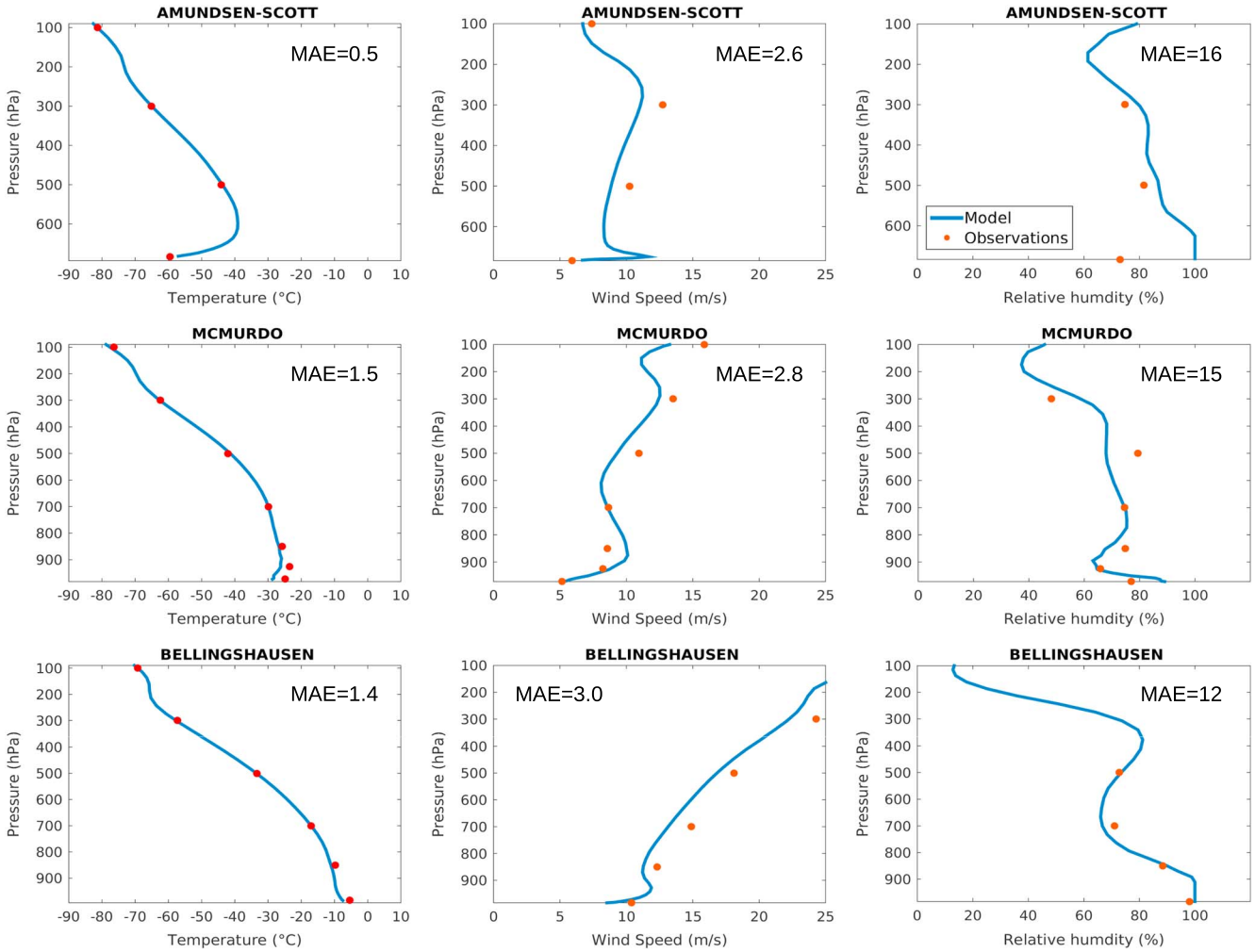

Figure 3. Same as Figure 2 but for the austral winter season (June-July-August).

3. Model Evaluation

3.1. Large-Scale and Upper Atmospheric Dynamics

A good simulation of the surface climate over the AIS relies on the correct representation of the large scale dynamical patterns. The atmosphere over the AIS is isolated from the midlatitudes by the circumpolar vortex that drives persistent westerly winds increasing in intensity with height throughout the troposphere (König-Langlo et al., 1998). Furthermore, the strength of the circumpolar vortex has a major impact on the AIS surface climate, including temperature and precipitation (van den Broeke & van Lipzig, 2004). An evaluation of the simulated large-scale flow over the AIS compared to ERA-Interim shows very good correspondences in the internal structure of the upper air atmosphere in both the austral summer and winter season (Figure S2 in the supporting information).

3.1.1. Temperature

The representation of the large scale atmospheric flow can further be investigated by performing a comparison with radiosoundings at 12 stations, which record the vertical structure of the atmosphere (Figure 1). The observational records are compared to the corresponding pixels of the grid of which the center is located less than 50 km from the measurement site. The average performance of the model versus the radiosoundings is visualized for both austral summer and winter for three stations located respectively inland (Amundsen Scott), at the coast (McMurdo), and the Antarctic Peninsula (Bellingshausen; Figures 2 and 3). The MAE is calculated as the average absolute difference between the monthly observed and modeled values and allows to investigate the temporal variability (see section 2.3). A full statistical comparison between the observations and the model for each pressure level for all 12 stations is available in Table S1 and S2 in the supporting

information. The MAE for all stations is calculated for both the austral summer and winter season at each individual pressure level. The 100-hPa level is discarded from this analysis and the calculation of MAE in Figures 2 and 3, since spectral nudging does not allow a fair comparison between the model and the IGRA data set, as these observations are assimilated in ERA-Interim, the driving GCM of the COSMO-CLM^2 simulation.

Generally, the COSMO-CLM^2 long-term simulation achieves an excellent average and temporal performance of the atmospheric temperature profile for all locations (MAE <= 1.5 °C). The temperature inversion on the Antarctic plateau is well simulated in both the austral summer and winter season, showing small biases. A quantitative comparison with the observations over Amundsen Scott presented in Hudson and Brandt (2005) shows adequate agreements. Inversion strength is calculated as the difference between the 2-m temperature and the maximum temperature in the profile. In austral winter, COSMO-CLM^2 simulates an average temperature inversion of 20 °C, which is close to the observed value of 22 °C in the observations of Hudson and Brandt (2005). In austral summer, the average inversion of 3 °C is also in line with observations (4 °C). COSMO-CLM^2 also simulates a small temperature inversion for the coastal station (Figures 2 and 3). This inversion is less pronounced in the observations for both the austral summer and winter season. For Bellingshausen, located at the northern part of the Antarctic Peninsula, the model correctly simulates no inversion. Lastly, the tropopause is clearly visible during the austral summer by a temperature minimum, the height of which is well simulated by COSMO-CLM^2, facilitated by the spectral nudging procedure (section 2.1).

3.1.2. Wind Speed

The AIS is overlaid by a cold high pressure system, isolated from the midlatitude atmosphere by the circumpolar vortex. This vortex is located at the top of the troposphere between 30°S and 60°S, implying high wind speeds at these levels for locations at the Antarctic Peninsula and the coast. A second maximum in wind speeds is present close to the surface, where a katabatic flow manifests originating from the mountain ridge and the Antarctic plateau toward the coast (Parish & Cassano, 2003). A maximum in wind speed is simulated close to the surface over inland stations during austral winter (Figure 3). This is identified as a low-level jet that is katabatically forced during stable conditions at nighttime and has been observed in several observational studies over the AIS (e.g., van As et al., 2006). Between the surface and the tropopause, the transition between the cyclonic vortex and the anticyclone at the surface leads to lower wind speeds (Parish & Bromwich, 2007). This typical S-shaped profile is less pronounced in the interior of the AIS compared to the coastal areas. The COSMO-CLM^2 simulation is able to correctly represent the vertical structure in the wind profile showing both the increase in wind speed near the surface driven by katabatic forcing and the wind speed maximum of the circumpolar vortex at approximately the 300-hPa height level. The model has a slight tendency to underestimate wind speed, mainly for heights between 700 and 300 hPa (Figures 2 and 3). MAE of approximately 3 m/s are found for each station, indicating the temporal variability is adequately simulated.

3.1.3. Relative Humidity

In contrast with moisture content, relative humidity is highly dependent on the temperature of the atmosphere. Biases in relative humidity can therefore not be attributed solely to biases in moisture content and might also be related to erroneous temperature representation. At the top of the atmospheric column in the stratosphere, both the COSMO-CLM^2 model and the observations show a strong decrease in the amount of available moisture between the 300- and 100-hPa height level in austral summer (Figures 2 and 3). This decrease in relative humidity is however not observed for Bellingshausen and other Russian stations. For these stations, a strong increase in relative humidity at the transition from the troposphere to the stratosphere is observed. This is attributed to the measurement technique used in Russian radiosoundings, which denote too high values for relative humidity at low pressure levels (Balagurov et al., 2006; Eckstein et al., 2015; Moradi et al., 2013). As such, Russian radiosounding relative humidity data above the 300-hPa height level is discarded from our analysis.

Relative humidity in the lower atmospheric layers is on average well represented at the coastal areas and the typical inversions are well simulated. For the inland stations nevertheless, there is a clear discrepancy between the radiosoundings and the COSMO-CLM^2 simulation, leading to an average overestimation larger than 20%. However, snowfall rates over the interior of the AIS are very low and snowfall occurs infrequently. In these areas, a large part of the accumulation originates from diamond dust, which occurs when a strong surface-based temperature inversion persists over the plateau (Schlosser et al., 2010). Vertical mixing

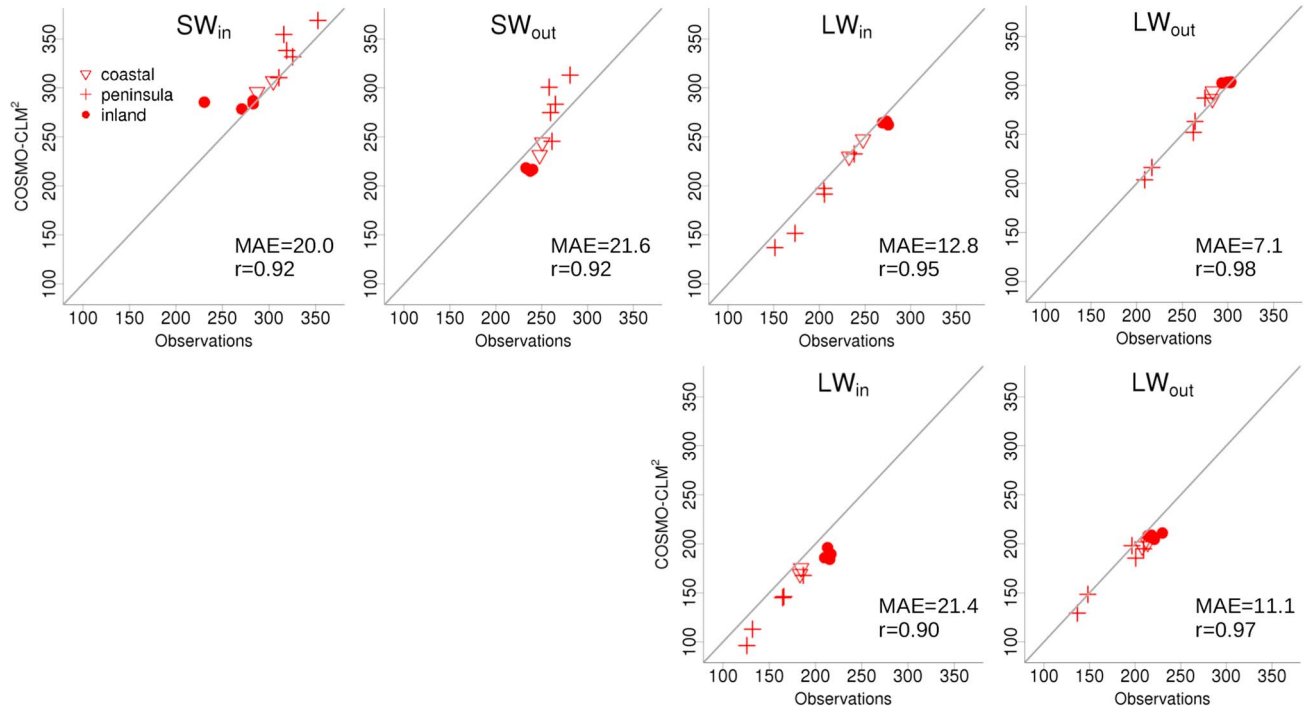

Figure 4. Comparison between radiative fluxes recorded by the AWSs and simulated in the COSMO-CLM^2 long-term simulation (W/m^2). SW_{in} (column 1), SW_{out} (column 2), LW_{in} (column 3), and LW_{out} (column 4) are considered. The austral summer season (December-January-February) is depicted in the top row, while the austral winter season (June-July-August) is shown in the bottom row. MAE denotes the mean absolute error, while *r* is the Pearson correlation coefficient, both calculated based on individual monthly observations. AWSs = automatic weather stations; SW = shortwave radiation; LW = longwave radiation

throughout the inversion layer causes these parts of the atmosphere to become supersaturated with respect to ice, so that small ice crystals can form producing diamond dust approximately 60% of the time at South Pole during austral winter (Walden et al., 2003). This does not only impact relative humidity in the inversion layer but also the simulated snowfall amounts in the interior of the AIS (see also section 3.3), as diamond dust significantly contributes to accumulation on the plateau (van de Berg et al., 2005). In the COSMO-CLM^2 simulation, the frequency of these diamond dust events is overestimated, attaining for too high values in simulated relative humidity values throughout the inversion layer. As this layer extents up to high altitudes for inland stations, the overestimation of relative humidity in the model can persist up to several hundreds of meters in altitude (Figure 3). Furthermore, radiosoundings are found to underestimate the humidity content in very cold conditions, attributing for part of the discrepancy (Genthon et al., 2010; Rowe et al., 2008; van As et al., 2006). MAE values for each location are generally high (10–20%) and highest values are found for the uppermost layers of the atmosphere (Tables S1 and S2). This shows the deficiency of the model to simulate upper-air temporal variability in relative humidity.

3.2. Surface Climate

3.2.1. Radiative Balance and Albedo

In order to correctly reproduce the surface climatology, the surface radiation balance should be considered, as it determines surface temperature and influences katabatic wind formation. Records of the radiative balance are available for 11 AWSs (Figure 4), located mainly on the margin of the AIS in Dronning Maud Land and the Antarctic Peninsula (Figure 1). Apart from the average values that are visualized in the figure, the MAE and Pearson correlation coefficient are calculated on monthly values in order to take the temporal variability into account.

The COSMO-CLM^2 simulation accurately represents the amount of incoming shortwave radiation (SW_{in}) for both the inland and coastal locations (apart from one inland station, considered an outlier). Over the Antarctic Peninsula, the discrepancy increases. These errors are likely related to the mountainous topography, leading to erroneous representation of diffuse shortwave radiation due to a smoothing of the domain by the model. For outgoing shortwave radiation (SW_{out}), the simulation spans a much wider range of values (210–300 W/m^2) than the observations (230–280 W/m^2), with a MAE of 20 W/m^2. Over the Antarctic

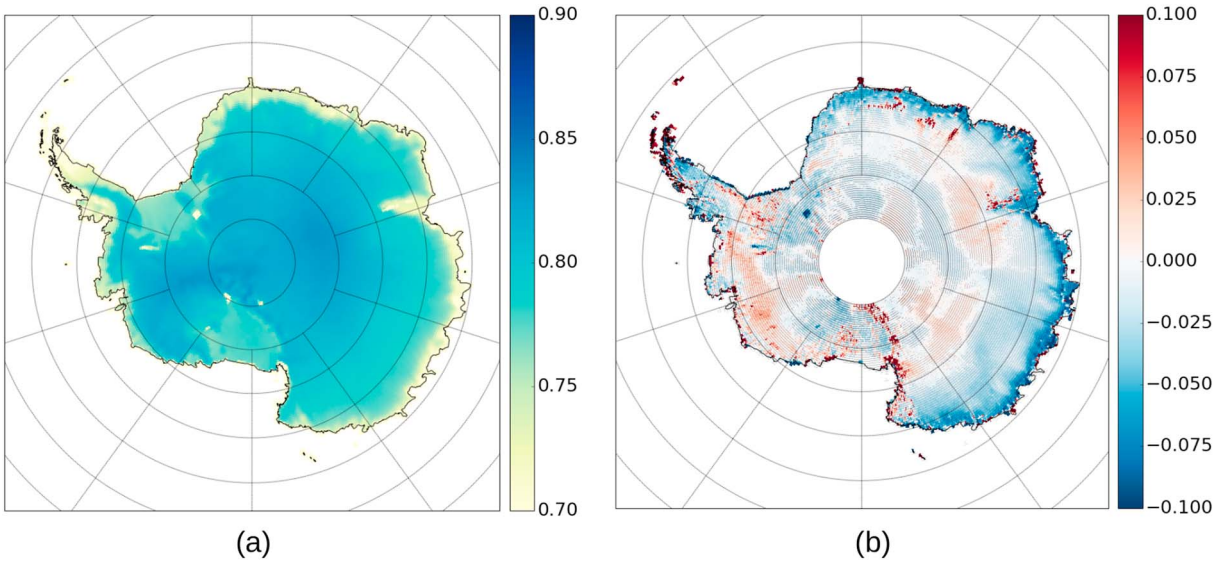

Figure 5. (a) Albedo climatology during austral summer (December-January-February) in COSMO-CLM^2 and (b) the absolute difference between the COSMO-CLM^2 simulation and the MODerate-resolution Imaging Spectroradiometer white sky albedo climatology. Hatched areas denote statistically significant differences, calculated using the two-sided Kolmogorov-Smirnov test on interannual differences in albedo values.

Peninsula, generally an overestimation of shortwave outgoing radiation is shown, which can be attributed to the overestimation in shortwave incoming radiation (Figure 4). Temporal variability is well simulated since MAE values are low (<20 W/m^2) and generally high correlation values are obtained. Apart from the AWSs, MODIS provides a continent-wide albedo product. This can directly be compared to the albedo parameter in the COSMO-CLM^2 simulation for the austral summer months. Biases in COSMO-CLM^2 are observed at the coast of East-Antarctica (Figure 5). In this region, the long-term model simulation underestimates the albedo by a factor up to 0.1, which leads to an underestimation of the reflected shortwave radiation (compare Figures 4 and 5) and therefore also impacts the temperature of the surface and the snow pack.

The average integrated snowfall input value in COSMO-CLM^2 (2,469 ±78 Gt/year), is slightly larger than the values of the MAR model (2,306 ±111) and RACMO2 (2,339 ±107; see Table 2 in Agosta et al., 2018). However, the albedo underestimation is essentially located at the coast, indicating that the COMSO-CLM^2 model produces too little precipitation at the coast, and increased precipitation amounts in the interior of the continent (see section 3.3).

The MODIS product shows lower albedo values over the ice shelves compared to the land-based ice sheet (Figure 5). This is well simulated in the long-term COSMO-CLM^2 simulation and is mainly attributed to the implementation of the Community Land Model and the modifications herein, allowing for a realistic representation of the ice shelves and their overlying snow pack. The surface albedo on the plateau of the AIS is well simulated, and no consistent biases are detected. The inland sites denoted in Figure 4 show an underestimation of the shortwave outgoing radiation. These stations are located in a zone with a small underestimation of the albedo compared to MODIS, explaining their bias (compare Figures 1 and 5). Over the Transantarctic Mountains and the Antarctic Peninsula, the long-term simulation overestimates the albedo. In reality large parts of the mountains are snow-free, leading to very low albedo values. In the model, these mountains are smoothed, allowing the snow pack to persist (Figure 5; van Lipzig, King, et al., 2004).

During the austral summer, both the incoming and outgoing longwave radiation (LW_{in} and LW_{out}, respectively) are well simulated in the model for all AWSs (Figure 4). In austral winter, however, there is a structural underestimation of the longwave incoming radiation in the model simulation, which equals on average 20 W/m^2. Based on cloud (phase) observations at the Princess Elisabeth station (71°57′S, 23°21′E; Figure 1), located in Dronning Maud Land, it is hypothesized that this could be attributed to an underestimation in the amount of (liquid-containing) clouds over the station during austral winter (Gorodetskaya et al., 2015). Clouds have a large radiative effect on the ice sheet and significantly contribute to the amount of incoming longwave radiation (Van Tricht et al., 2016). Furthermore, state-of-the-art climate models have substantial biases in cloud representation over polar regions (Lenaerts et al., 2017). During the austral winter of 2015,

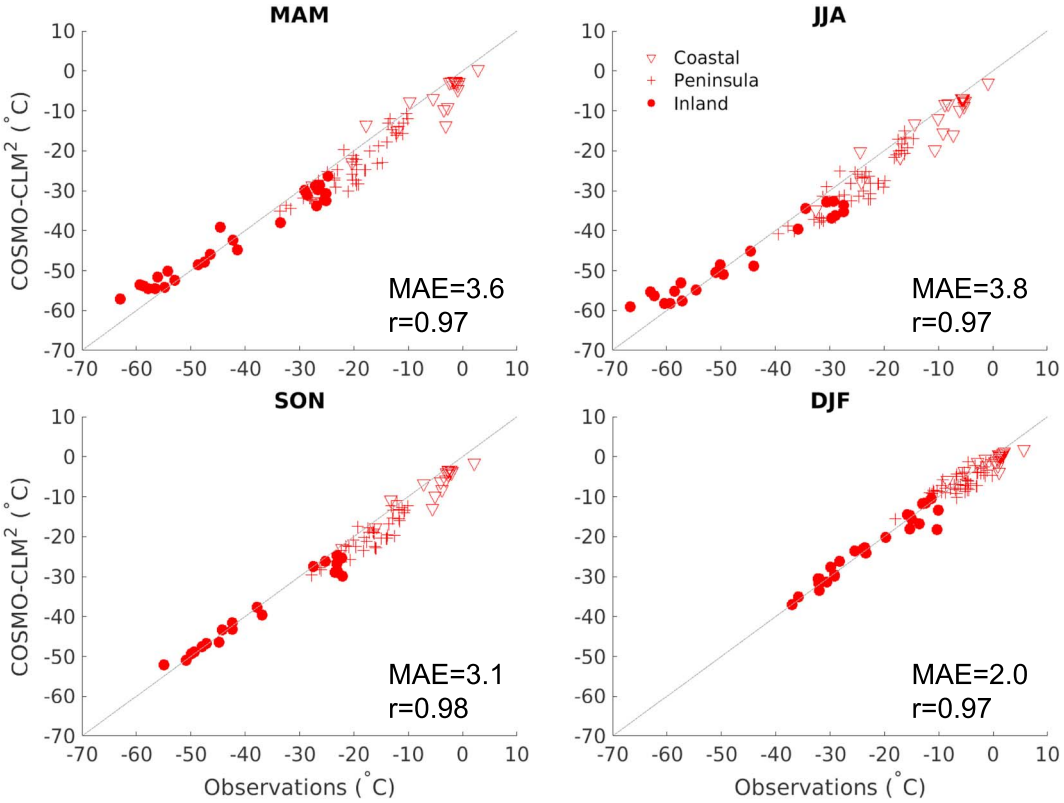

Figure 6. Seasonally averaged ground-based temperature observations (°C) compared to the corresponding pixel in COSMO-CLM^2. MAE denotes the mean absolute error, while *r* is the Pearson correlation coefficient, both calculated based on individual monthly observations. MAM = March-April-May; JJA = June-July-August; SON = September-October-November; DJF = December-January-February.

ceilometer observations are available at the Princess Elisabeth station. This instrument can detect cloud base heights and is able to make a distinction between liquid and ice clouds using the approach of Gorodetskaya et al. (2015) and Van Tricht et al. (2014). In austral winter 2015, the ceilometer observed overcast conditions 77% of the time. In 46% of the cases these clouds contained liquid droplets. In the COSMO-CLM^2 simulation, cloudy conditions were limited to 52% during the season. Moreover, liquid clouds were almost nonexistent (<1% of the time). This probably contributes to the longwave downward biases during austral winter (Figure 4).

3.2.2. Temperature

In general, near-surface temperatures have a MAE in the range of 2–4 °C compared to observations and attain very high correlation coefficients, indicating good average and temporal performance. For coastal areas, temperatures are slightly underestimated by the COSMO-CLM^2 model. This feature is persistent throughout the year, apart from the austral summer, during which the temperature match is excellent (Figure 6). Coastal areas are however characterized by slightly too low albedo values (Figure 5 and section 3.2.1). As such, the general cold bias might for this season be compensated by a too large absorption of shortwave radiation. Temperatures on the plateau of the AIS are well represented during austral summer (MAE < 2 °C), but are slightly overestimated by 3–4 °C during June-July-August and March-April-May for locations on the Antarctic plateau (Table S6 in the supporting information). During these seasons, the model is not capable to fully cover the temperature range that is present over the AIS: an overestimation of temperatures is present over the highest (coldest) locations of the AIS, as extremely stable boundary layer conditions are difficult to represent in the model (Figure 7).

Temperatures over the ice shelves are reasonably well represented by the COSMO-CLM^2 model. This is clearly visible for the Ross Ice Shelf, for which many observations are available (Figure 7). Temperatures over this ice shelf are influenced by strong surface winds of both katabatic and geostrophic origin (van den Broeke & van Lipzig, 2003), as they are capable of transporting cold air masses from inland regions toward

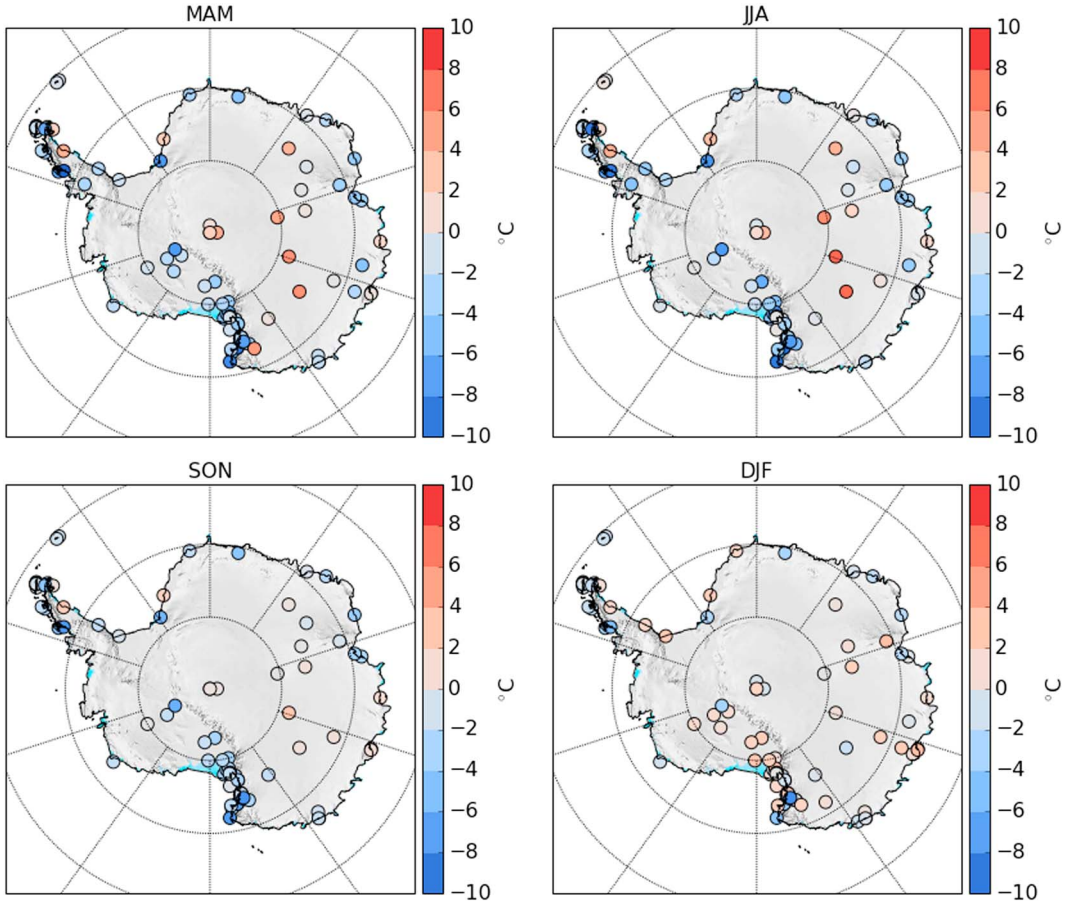

Figure 7. Temperature bias between seasonally averaged ground-based observations and the corresponding pixel in COSMO-CLM^2. The background is provided by the ETOPO1 global relief model (Amante & Eakins, 2009). MAM = March-April-May; JJA = June-July-August; SON = September-October-November; DJF = December-January-February.

these lower locations. A correct representation of the surface temperature is therefore only possible when these winds are correctly simulated. By modifying the roughness length of snow and the representation of stability in the atmospheric boundary layer (see section 2.2), a correct representation of the atmospheric boundary layer and the surface temperature and wind field is obtained.

The Antarctic Peninsula is characterized by a highly variable topography and distinctly different responses between the east and west side of the barrier to prevailing westerlies are observed (van Lipzig et al., 2008). A strong relation between temperature and elevation for the Antarctic Peninsula was shown by van Wessem et al. (2015). The COSMO-CLM^2 model however overestimates the temperature contrast between the leeward and windward side. This deficiency can be attributed to an inadequate representation of the foehn winds and the interactions with the topography and the surrounding air masses. When the westerly winds rise over the mountain ridge of the Antarctic Peninsula, several interactions with the environment take place, that is, radiative heating, latent heat release, precipitation on the leeward side of the mountain and turbulent mixing (Elvidge & Renfrew, 2016). In case one of these processes is not well represented, for example, due to a smoothing of the topography in the model, an erroneous representation of temperatures on the windward side of the Antarctic Peninsula is obtained. The cold bias on the windward side is also substantial and leads to biases up to 3 °C (Table S6 in the supporting information). This can be attributed to the coarse horizontal resolution of the COSMO-CLM^2 model. The stations are located near the coast, but in the highly variable topography of the Antarctic Peninsula, they might be compared to pixels with higher topography, leading to a cold bias.

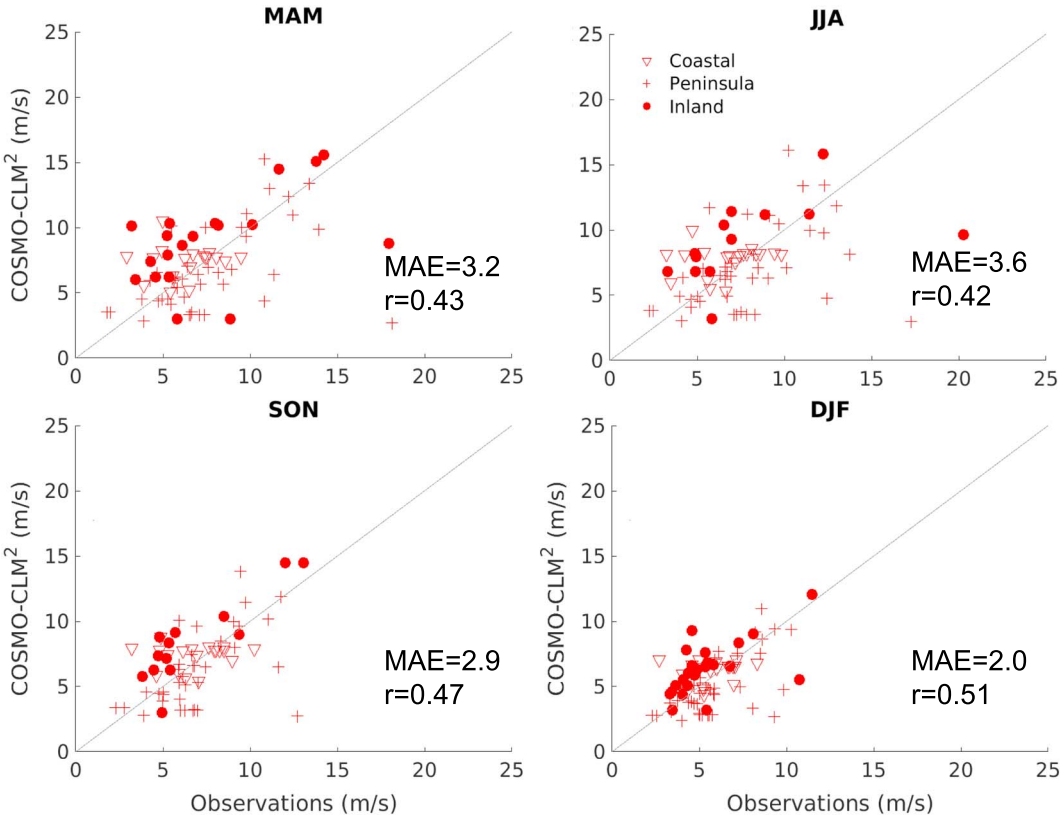

Figure 8. Seasonally averaged ground-based wind speed observations (m/s) compared to the corresponding pixel in COSMO-CLM^2. MAE denotes the mean absolute error, while *r* is the Pearson correlation coefficient, both calculated based on individual monthly observations. MAM = March-April-May; JJA = June-July-August; SON = September-October-November; DJF = December-January-February.

3.2.3. Wind Speed

The near-surface wind field is an important meteorological element over the AIS and is mainly determined by diabatic cooling of near-surface air close to the slopes of the continent, and the orography of the AIS, which induce katabatic slope flows (Parish & Bromwich, 1986, 1987; Parish & Cassano, 2003; van den Broeke & van Lipzig, 2003; van Lipzig, Turner, et al.,2004). A cold high pressure system is located over the continent, feeding the katabatic flows from the interior plateau toward the escarpment of the coast (van Lipzig, Turner, et al.,2004). Apart from the katabatic flow, the large-scale flow at the coastal margins of the AIS is dominated by the circumpolar vortex, that is, cyclonic activity near the coast of the AIS allowing for the transport of moisture and air from midlatitudes to the AIS at high wind speeds (Gorodetskaya et al., 2014; Souverijns et al., 2017, 2018).

Near-surface wind speeds are generally overestimated by COSMO-CLM^2 in the AIS interior by 2–5 m/s (Figures 8 and 9). This might be related to the low roughness length coefficient, representative for glazed areas and leading to higher wind speeds. However, at the coastal margins, the performance improves, showing smaller biases (MAE <3 m/s) mainly in the austral summer period (Table S6 in the supporting information). A large variability in the performance of wind speed representation in COSMO-CLM^2 is present for the coastal stations and over the Antarctic Peninsula (Figure 8). These measurement areas are often located in highly variable topography near the ice sheet margins not representative for the ice sheet surface. On the local scale, stations might be shielded from katabatic flow or located in a wind confluence zone. As the resolution of the simulation is too coarse to represent this small-scale variability in topography, an erratic pattern of biases is expected, leading to correlation coefficients between 0.4 and 0.6.

3.2.4. Relative Humidity

For five inland stations (located at the edge of the plateau between 1,000 and 3,000 m above sea level; see also Figure 1) long-term humidity measurements are available at 2 m a.g.l. Relative humidity near the surface is generally underestimated by 10–20% by the COSMO-CLM^2 simulation compared to AWS observations

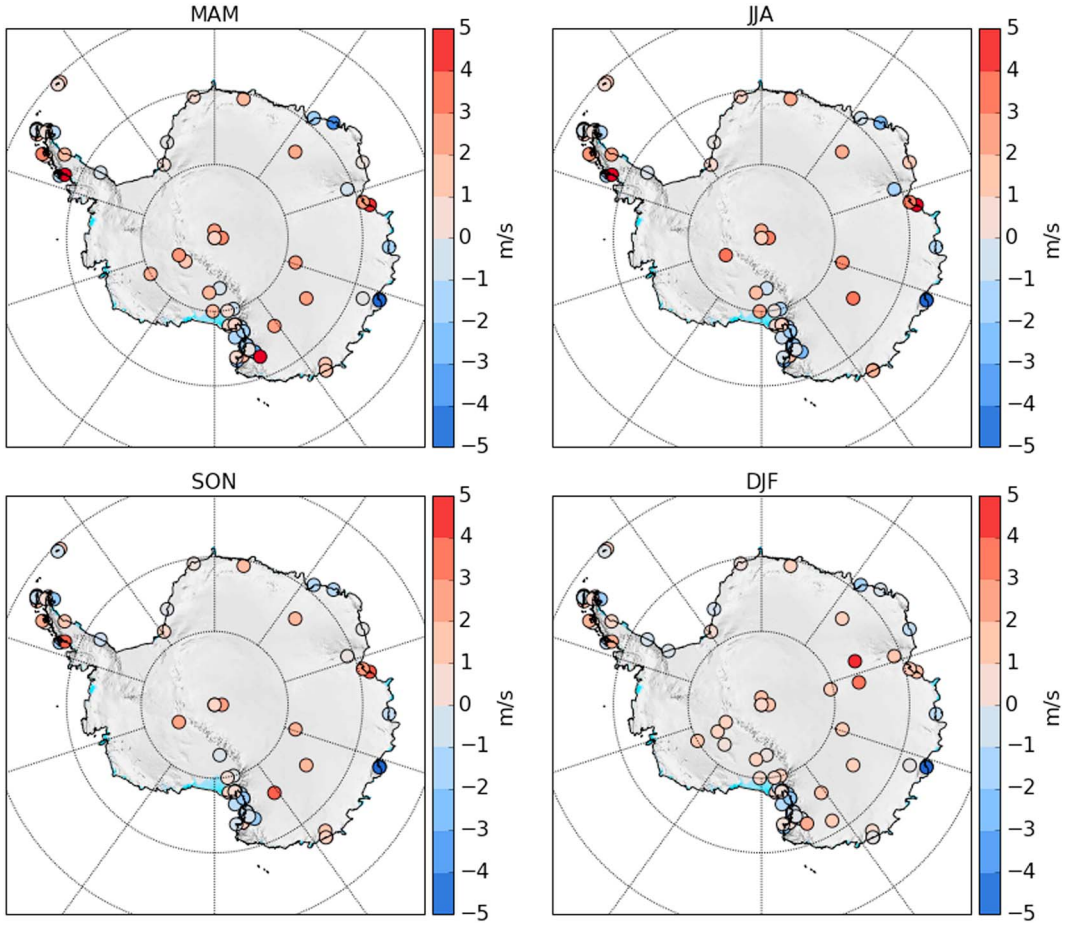

Figure 9. Wind speed bias between seasonally averaged ground-based observations and the corresponding pixel in COSMO-CLM^2. The background is provided by the ETOPO1 global relief model (Amante & Eakins, 2009). MAM = March-April-May; JJA = June-July-August; SON = September-October-November; DJF = December-January-February.

located in Dronning Maud Land and the Antarctic Peninsula (Figures 1 and 10). This stands in contrast with the results from section 3.1.3, where an overestimation of the relative humidity in the lowest layers of the atmosphere was observed for observations located on the plateau (Figures 2 and 3). In contrast with the plateau, the AWSs are not located in areas with high diamond dust production in the model, explaining the lower observed relative humidity values.

3.2.5. Temporal Variability

Apart from simulating the climatology correctly, it is also important to simulate meteorological variability. This is illustrated for stations located on the coast, inland and the Antarctic Peninsula (Figure 11). The seasonal cycle present in temperature and wind speed is adequately simulated and is consistent with the results obtained above. A consistent underestimation of temperature is present for the coastal Mawson station, which is a common feature that is also detected in Figures 6 and 7. Regarding wind speed, the model has a tendency to overestimate wind speeds for most of the AIS, which can be observed for the Amundsen Scott station (2 m/s on average) and for the coastal station Mawson during austral winter. Furthermore, the yearly variability in monthly temperature and wind speed is adequately simulated by COSMO-CLM^2. This is nicely illustrated for near-surface temperature where in austral winter, the spread in observed and modeled values is much larger than in austral summer for all three stations. Wind speed values at the coastal Mawson station also are characterized by an interannual variability, which is also nicely captured by the model. For relative humidity, the model strongly underestimates observed values for all stations (Figure 11). Furthermore, for the coastal station and the station located on the Antarctic Peninsula, a reversed seasonal cycle is modeled and the interannual variability is not well simulated. This indicates that problems persist regarding the representation of humidity near the surface and that more work regarding this issue is necessary.

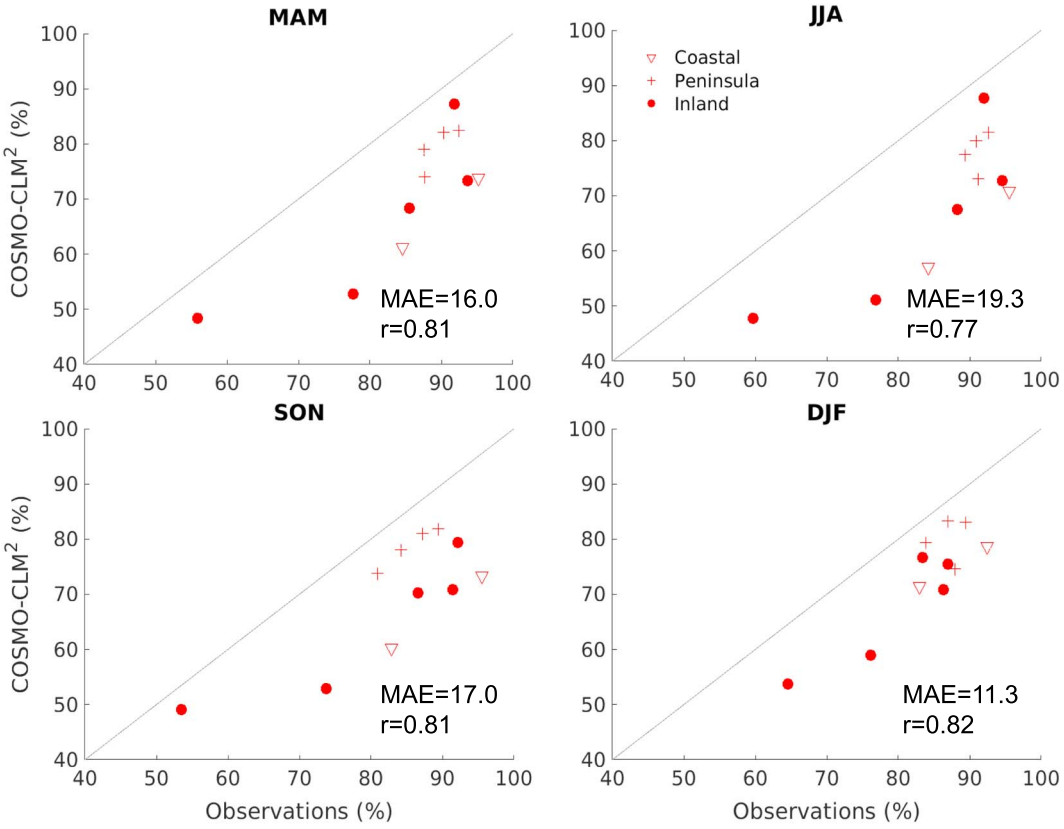

Figure 10. Seasonally averaged ground-based relative humidity observations (%) compared to the corresponding pixel in COSMO-CLM^2. MAE denotes the mean absolute error, while *r* is the Pearson correlation coefficient, both calculated based on individual monthly observations. MAM = March-April-May; JJA = June-July-August; SON = September-October-November; DJF = December-January-February.

3.3. SMB

SMB is simplified in our COSMO-CLM^2 simulation to snowfall minus surface sublimation. However, other processes also play a role in (local) SMB. Wind-driven snow transport is an important process in redistributing snow over the ice sheet (Souverijns et al., 2018) and in the creation of blue ice zones (Takahashi, 1988). But integrated over the ice sheet, the importance of snow removal by erosion is estimated to be 2 orders of magnitude smaller than surface sublimation (Déry & Yau, 2002). Blowing snow sublimation occurs when the ambient air in which suspended snow particles float is undersaturated (Schmidt, 1982). This term is capable to remove 10% of the accumulated snowfall (Déry & Yau, 2002) but has a large spatial variability (Thiery et al., 2012). As its influence is substantial, this needs to be considered in the interpretation of the model results. However, for our analysis regarding large areas over the AIS, the simplification has probably limited effect (Agosta et al., 2018; van Wessem et al., 2018).

Generally, a good agreement is found between the observational SMB and the integrated mean SMB in the long-term COSMO-CLM^2 simulation for the 1987–2010 period for most of the locations higher than 500 m a.s.l. (Figure 12). The SMB is however underestimated for the lowest elevation areas, that is, the ice shelves and the coast. There, the displacement and sublimation of snow particles, not represented in the model, can explain most of the variations in the local SMB, visible in the observational database, and not captured in the model.

When investigating the spatial pattern of the COSMO-CLM^2 simulated SMB with the reconstruction based on ice cores and ERA-Interim (Medley & Thomas, 2019), a significant underestimation of the SMB is found for most of the coastal sites including the Antarctic Peninsula (Figures 13 and S3 in the supporting information). This underrate of the SMB at coastal sites is attributed to both an underestimation of snowfall and the simplification of modeled SMB to snowfall minus sublimation. The underestimation of snowfall is larger for the Antarctic Peninsula, and affects the albedo and thereby the surface energy balance (section 3.2.1). The

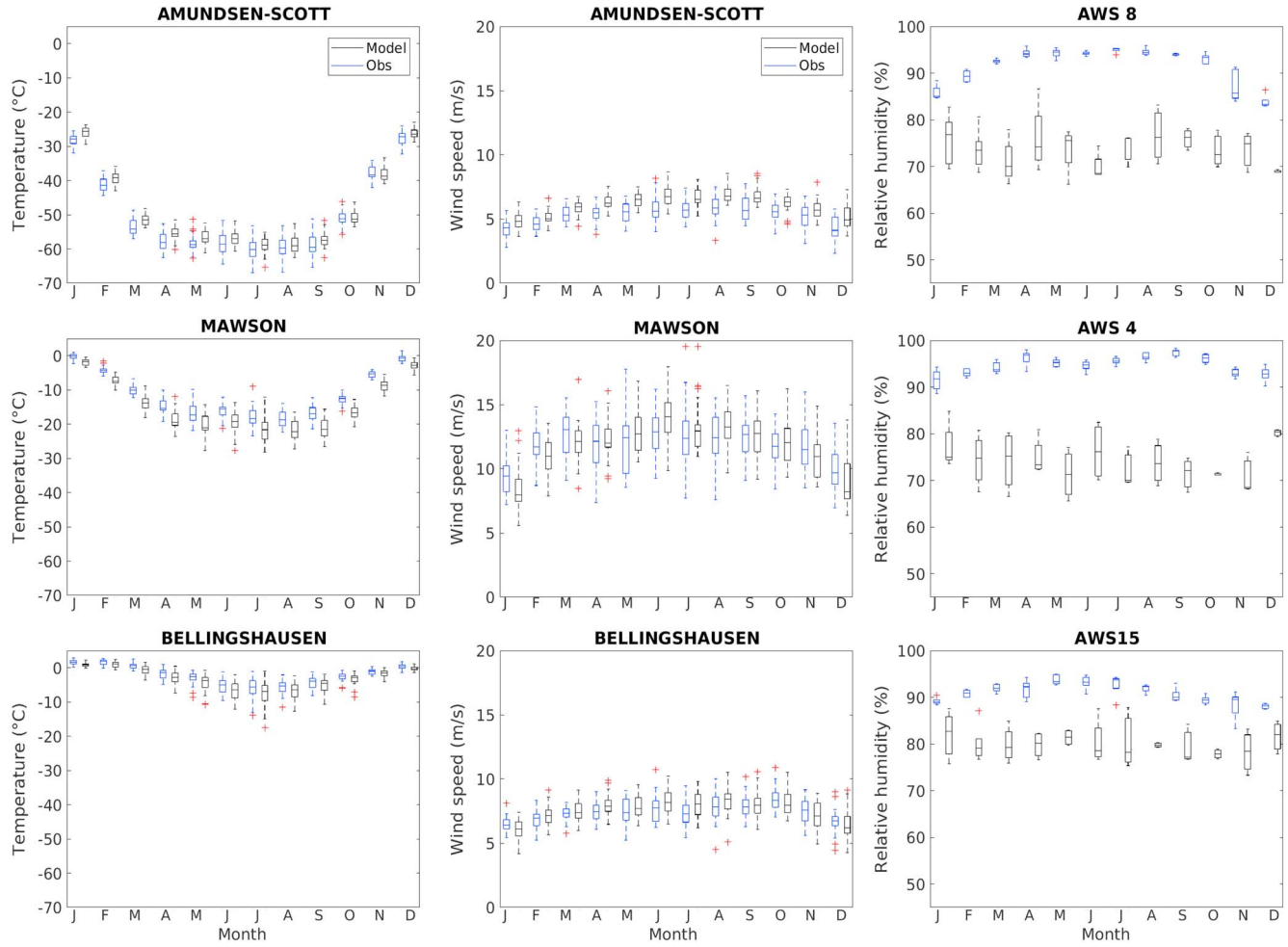

Figure 11. Seasonal cycle and monthly variability of near-surface temperature, wind speed, and relative humidity for inland stations (first row), coastal stations (second row), and stations located on the Antarctic Peninsula (third row). Different stations were chosen for relative humidity due to the unavailability of relative humidity measurements near the surface at Amundsen Scott, Mawson, and Bellingshausen. Temperature and relative humidity are obtained at 2 m above ground level, while wind speed is recalculated to this level using the approach of Sanz Rodrigo (2011) as described in section 2.3.

neglect of surface melt and snowdrift processes, especially active on the ice shelves and coastal areas, leads to local underestimation and overestimation of the modeled SMB.

Table 1 contains the integrated mean values for SMB (snowfall minus precipitation) per sector (defined on the basis of Zwally et al. (2012), as well as the subdivision used throughout this paper [interior, coast, and ice shelves]). The range of the COSMO-CLM^2 results are in the range of other state-of-the-art models. While the total snowfall amount is slightly overestimated in comparison to MAR (Agosta et al., 2018) and RACMO2 (van Wessem et al., 2018) by a bit more than 100 GT/year (for a full overview of RACMO2.0 and MAR results, see Table 2 in Agosta et al., 2018), the sublimation component is 2 to 5 times more efficient than in the other models, leading to a total under-estimation of the integrated mean SMB. COSMO-CLM^2 values over the grounded ice sheet are within the range of the state-of-the-art models, but while East Antarctica and West Antarctic SMB values are overestimated, the Antarctic Peninsula SMB is underestimated. Since the surface sublimation ratio (9%) is lower at the peninsula than in other sectors, this highlights the snowfall bias: an underestimation at the coastal areas (including the peninsula) and an overestimation inland. Considering that the integrated mean surface sublimation is fairly stable over the time period, the variability of SMB is attributed to snowfall interannual variability (see Figure S3).

An evaluation of the temporal variability of mass changes in COSMO-CLM^2 is executed compared to GRACE for Dronning Maud Land. The cumulative mass change line increases largely in 2009, and in a more limited extent in 2011, in both the model and the GRACE-derived mass changes (Figure 14). In 2009, especially,

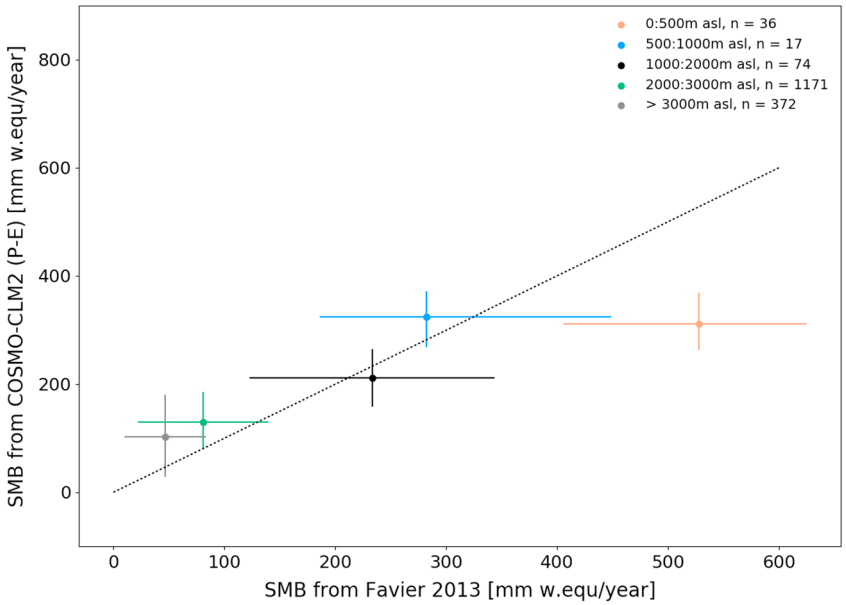

Figure 12. Surface mass balance estimates obtained by Favier et al. (2013) and Medley and Thomas (2019) for the period 1987–2010 compared to the surface mass balance reconstruction of COSMO-CLM^2 (described in section 2.3). The observations are binned in different height classes. The dot denotes the mean value of the height bin, while the error bars denote the 10th and 90th percentiles of the data points for each class (horizontal) and the corresponding model (vertical). SMB = surface mass balance.

the two lines are perfectly overlaid, and a very limited bias is present in 2011. The good agreement between both lines is however not attributable to a perfect spatial match in SMB between the model and observations but to a compensation of areas with overestimation and underestimation in SMB within Dronning Maud Land (Figure 13). These features are mainly observed in mountainous areas, featuring large topographical differences, attributing the misplacement of SMB to an erroneous representation of orographic precipitation. Furthermore, areas with a higher altitude often have a slight overestimation in SMB, compensating for the underestimation of SMB at coastal areas.

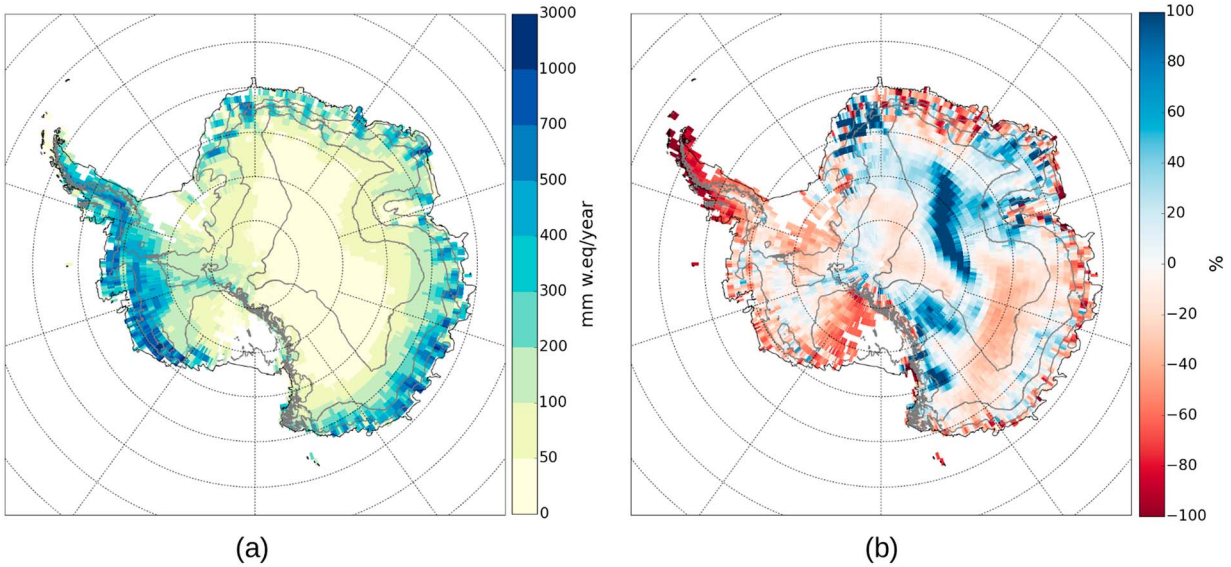

Figure 13. (a) Surface mass balance reconstruction in COSMO-CLM^2 based on the difference between snowfall and evaporation (sublimation) and (b) the relative difference compared to the reconstruction presented in Medley and Thomas (2019), for the model period. Contours denote elevation with an interval of 1,000 m.

Table 1
Integrated Modeled SMB, Snowfall, and Surface Sublimation on Average Over the 1987–2016 Time Period, in Gigaton per Year ± One Standard Deviation

Basin	SMB (Gt/year)	Snowfall (Gt/year)	Surface sublimation (Gt/year)
Total ice sheet	2,177 ±80	2,469 ±78	292 ±10
Grounded ice sheet	2,107 ±76	2,386 ±78	278 ±10
East Antarctica	1,235 ±86	1,430 ±89	195 ±9
West Antarctica	694 ±53	759 ±54	65 ±4
Peninsula	178 ±15	197 ±15	18 ±1
Coast	1,254 ±563	1,276 ±562	219 ±7
Interior	925 ±52	990 ±53	66 ±5
Ice shelves	69 ±25	83 ±25	14 ±0.5

Note. The delimitation between the Peninsula and East and West Antarctica is made upon the basins defined by Zwally et al. (2012). SMB = surface mass balance.

The representation of the SMB showed reasonable agreements compared to observations for most regions apart from the coast and the Antarctic Peninsula, for which biases higher than 50% were found. For a small inland zone, a high overestimation is found. This can be attributed to large precipitation events attributing to extreme precipitation rates, not present in the model (see Figure S3) and the constant under-estimation of precipitation over the ice shelves, the coastal area and the Antarctic Peninsula. For these areas, improvements toward the future are necessary to achieve more accurate representations. The inclusion of an improved tuning of the parameters in the cloud microphysical scheme, the representation of blowing snow, and an improved albedo parametrization are crucial to constrain ice shelves and coastal SMB biases and to reach the performance of, for example, RACMO2 (biases limited to 20%; van Wessem et al., 2018; Wang et al., 2016). However, the timing and magnitude of the snowfall anomalies (Figure 14) are well reproduced by COSMO-CLM^2 and are comparable to RACMO2 performance (Lenaerts et al., 2013). In addition, the cumulative mass change of COSMO-CLM^2 in Dronning Maud Land lies within the uncertainty of GRACE.

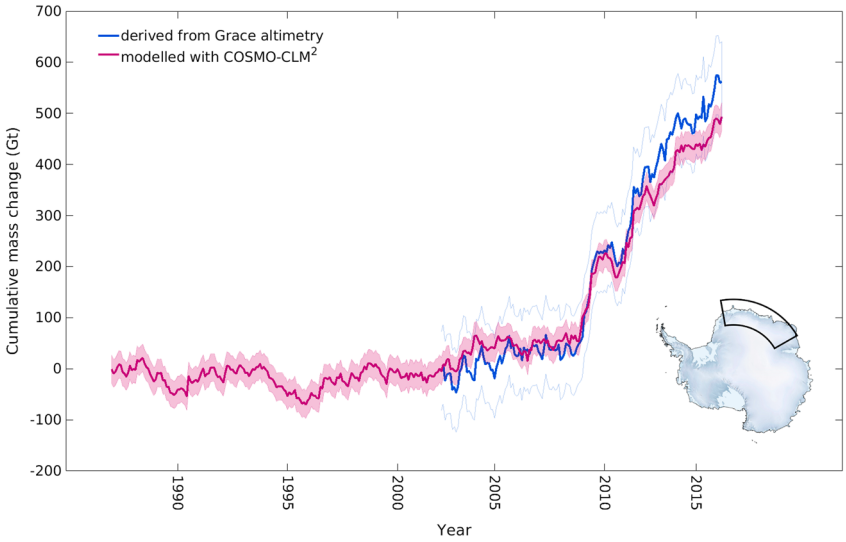

Figure 14. Cumulative mass change derived from GRACE altimetry over the 2002–2016 period and COSMO-CLM^2 for the Dronning Maud Land region (see inset). The COSMO-CLM^2 value is shown as the cumulative anomaly of the monthly surface mass balance with respect to the period 1983–2002. The envelope represents uncertainties of GRACE and COSMO-CLM^2 simulations. The uncertainty on the modeled COSMO-CLM^2 cumulative surface mass balance anomalies is computed based on the choice of reference period (1983–2002, prior to GRACE measurements), following the method described in van den Broeke et al. (2009). GRACE = Gravity Recovery and Climate Experiment.

4. Conclusions

The climate over the AIS highly influences its SMB which in turn is strongly linked with global sea level rise. As meteorological observations over the AIS are scarce, RCMs are excellent tools to investigate the climate of this continent. In the last decades, RCMs have been adapted to represent the climate over the AIS. However, regional climate modeling over the AIS is restricted to a limited number of simulations by a few, usually hydrostatic, models. In this study, the nonhydrostatic COSMO RCM is applied to the AIS after several adaptations to the model were made. The model is coupled to the Community Land Model (COSMO-CLM^2), adapted for AIS surface representation, to improve snow pack representation and to account for firn processes. Moreover, the roughness length of snow was modified, the turbulence scheme was altered to account for stable boundary layer representation, upper air variables were nudged to the driving global model, and the two-moment cloud-precipitation scheme was adapted to better represent cloud microphysical properties in pristine conditions prevailing over the AIS. A 30-year (1987–2016) hindcast simulation was performed and evaluated against a compilation of observational records consisting of long-term ground-based and upper-air meteorological observations, AWSs, satellite records, stake measurements, and ice cores, unprecedented for current model evaluation over the AIS. All observations presented above are publicly available (see section 2.3).

An adequate representation of upper air temperature, wind speed and pressure patterns was achieved, showing confidence in the large-scale dynamics of the COSMO-CLM^2 model. Relative humidity is also well represented. Over the Antarctic plateau, the frequency of low-intensity snowfall is however overestimated, leading to high values of relative humidity.

The surface climate is well simulated by the COSMO-CLM^2 long-term simulation, with limited biases in the near-surface meteorological variables, that is, temperature, wind speed, and relative humidity. A consistent underestimation of relative humidity values at the edge of the Antarctic plateau and the coast is however simulated by COSMO-CLM^2. This is potentially attributed to the absence of blowing snow in the model, which has the ability to increase relative humidity due to sublimation of suspended snow particles.

The radiative balance at the surface of the AIS is accurately represented in the COSMO-CLM^2 model. A lack of (liquid) clouds over the ice sheet leads to an underestimation of the longwave downward radiation in austral winter, while biases in shortwave radiation were attributed to topographical smoothing in the model and an underestimation of the albedo. A comparison with the MODIS albedo product attained a good performance over the plateau but shows an underestimation at the coastal sites of East Antarctica. Reconstructions of the SMB of the AIS indicate a correct representation of the large-scale accumulation patterns over the AIS but an underestimation of the amount of snowfall at the coastal sites and the Antarctic Peninsula. For inland sites, a good representation is achieved, apart from some limited locations which show an overestimation of the accumulated snow amount. Improvements in the representation of albedo, cloud cover, drifting snow, and coastal precipitation are therefore future priorities for the polar version of COSMO-CLM^2.

Generally, the COSMO-CLM^2 model is capable of adequately simulating the Antarctic climate. It therefore adds as an extra member to the ensemble of RCMs over the AIS needed by the international COordinated Regional Downscaling EXperiment (CORDEX) project and the Intergovernmental Panel on Climate Change fifth assessment report. Furthermore, the application of COSMO-CLM^2 over the AIS contributes to POLAR-CORDEX and the CORDEX-CORE initiative, aiming to apply the same set of models to all CORDEX regions (Giorgi & Gutowski, 2016; Gutowski et al., 2016). In future, the COSMO-CLM^2 model will be used to perform historical simulations and climate projections over the AIS.

Acknowledgments
This work was supported by the Belgian Science Policy Office (BELSPO; grant BR/143/A2/AEROCLOUD) and the Research Foundation Flanders (FWO; grant G0C2215N). COSMO-CLM is the community model of the German regional climate research jointly further developed by the CLM-Community. The computational resources and services used in this work were provided by the VSC (Flemish Supercomputer Center), funded by the Research Foundation-Flanders (FWO) and the Flemish Government-Department EWI. Martijn Oldenhof and Jan Ooghe (KU Leuven) are acknowledged for their support in the installation of the COSMO-CLM^2 model. Leonardus van Kampenhout (Institute for Marine and Atmospheric Research Utrecht) is thanked for his advice in the application of the Community Land Model. We thank Wim Boot, Carleen Reijmer, and Michiel van den Broeke (Institute for Marine and Atmospheric Research Utrecht) for the development of the automatic weather stations, technical support, and raw data processing. Part of the observational data were obtained from "MeteoClimatological Observatory at Mario Zucchelli Station and Victoria Land" of PNRA (http://www.climantartide.it) and the Australian Antarctic Division Glaciology Program. The authors appreciate the support of the University of Wisconsin-Madison automatic weather station Program for the data set, data display, and information, NSF grant ANT-1543305. The COSMO-CLM^2 monthly output of the key variables described in the paper is open-access available (https://doi.org/10.5281/zenodo.2539147).

References

Agosta, C., Amory, C., Kittel, C., Orsi, A., Favier, V., Gallée, H., et al. (2018). Estimation of the Antarctic surface mass balance using MAR (1979–2015) and identification of dominant processes. *The Cryosphere Discussions*. https://doi.org/10.5194/tc-2018-76

Agosta, C., Favier, V., Krinner, G., Gallée, H., Fettweis, X., & Genthon, C. (2013). High-resolution modelling of the Antarctic surface mass balance, application for the twentieth, twenty first and twenty second centuries. *Climate Dynamics*, *41*, 3247–3260. https://doi.org/10.1007/s00382-013-1903-9

Amante, C., & Eakins, B. (2009). ETOPO1 1 Arc-Minute Global Relief Model: Procedures. Data sources and analysis. https://doi.org/10.1594/PANGAEA.769615

Anderson, P. S. (1994). A method for rescaling humidity sensors at temperatures well below freezing. *Journal of Atmospheric and Oceanic Technology*, *11*, 1388–1391. https://doi.org/10.1175/1520-0426(1994)011<1388:AMFRHS>2.0.CO;2

Balagurov, A., Kats, A., Krestyannikova, N., & Schmidlin, F. (2006). WMO radiosonde humidity sensor intercomparison (Instruments and observing methods report No. 85 WMO/TD-No. 1305, Tech. Rep.) Geneva, Switzerland: WMO.

Boening, C., Lebsock, M., Landerer, F., & Stephens, G. (2012). Snowfall-driven mass change on the East Antarctic Ice Sheet. *Geophysical Research Letters*, *39*, L21501. https://doi.org/10.1029/2012GL053316

Bracegirdle, T. J., & Marshall, G. J. (2012). The reliability of Antarctic tropospheric pressure and temperature in the latest global reanalyses. *Journal of Climate*, *25*, 7138–7146. https://doi.org/10.1175/JCLI-D-11-00685.1

Bromwich, D. H., Otieno, F. O., Hines, K. M., Manning, K. W., & Shilo, E. (2013). Comprehensive evaluation of polar weather research and forecasting model performance in the Antarctic. *Journal of Geophysical Research: Atmospheres*, *118*, 274–292. https://doi.org/10.1029/2012JD018139

Buzzi, M., Rotach, M. W., Raschendorfer, M., & Holtslag, A. A. M. (2011). Evaluation of the COSMO-SC turbulence scheme in a shear-driven stable boundary layer. *Meteorologische Zeitschrift*, *20*(3), 335–350. https://doi.org/10.1127/0941-2948/2011/0050

Cassano, J. J., Parish, T. R., & King, J. C. (2001). Evaluation of turbulent surface flux parameterizations for the stable surface layer over Halley, Antarctica. *Monthly Weather Review*, *129*, 26–46. https://doi.org/10.1175/1520-0493(2001)129<0026:EOTSFP>2.0.CO;2

Cerenzia, I., Tampieri, F., & Tesini, M. S. (2014). Diagnosis of turbulence schema in stable atmospheric conditions and sensitivity tests. *COSMO Newsletter*, *14*, 1–11.

Chaubey, J. P., Krishna Moorthy, K., Suresh Babu, S., & Nair, V. S. (2011). The optical and physical properties of atmospheric aerosols over the Indian Antarctic stations during Southern Hemispheric summer of the International Polar Year 2007–2008. *Annales Geophysicae*, *29*, 109–121. https://doi.org/10.5194/angeo-29-109-2011

Davin, E. L., Stockli, R., Jaeger, E. B., Levis, S., & Seneviratne, S. I. (2011). COSMO-CLM2: A new version of the COSMO-CLM model coupled to the Community Land Model. *Climate Dynamics*, *37*, 1889–1907. https://doi.org/10.1007/s00382-011-1019-z

Dee, D. P., Uppala, S. M., Simmons, A. J., Berrisford, P., Poli, P., & Kobayashi, S. (2011). The ERA-Interim reanalysis: Configuration and performance of the data assimilation system. *Quarterly Journal of the Royal Meteorological Society*, *137*(656), 553–597. https://doi.org/10.1002/qj.828

Déry, S. J., & Yau, M. K. (2002). Large-scale mass balance effects of blowing snow and surface sublimation. *Journal of Geophysical Research*, *107*(23), 4679. https://doi.org/10.1029/2001JD001251

Dethloff, K., Glushak, K., Rinke, A., & Handorf, D. (2010). Antarctic 20th century accumulation changes based on regional climate model simulations. *Advances in Meteorology*, *2010*(327), 172. https://doi.org/10.1155/2010/327172

Durre, I., Xungang, Y., Vose, R. S., Applequist, S., & Arnfield, J. (2018). Integrated Global Radiosonde Archive (IGRA). Version 2. https://doi.org/10.7289/V5x63K0Q

Ebner, L., Heinemann, G., Haid, V., & Timmermann, R. (2014). Katabatic winds and polynya dynamics at Coats Land, Antarctica. *Antarctic Science*, *26*(3), 309–326. https://doi.org/10.1017/S0954102013000679

Eckstein, J., Schmitz, S., & Ruhnke, R. (2015). Reaching the lower stratosphere: Validating an extended vertical grid for COSMO. *Geoscientific Model Development*, *8*, 1839–1855. https://doi.org/10.5194/gmd-8-1839-2015

Elvidge, A., & Renfrew, I. A. (2016). The causes of foehn warming in the lee of mountains. *Bulletin of the American Meteorological Society*, *97*, 455–466. https://doi.org/10.1175/BAMS-D-14-00194.1

Favier, V., Agosta, C., Parouty, S., Durand, G., Delaygue, G., Gallée, H., et al. (2013). An updated and quality controlled surface mass balance dataset for Antarctica. *The Cryosphere*, *7*, 583–597. https://doi.org/10.5194/tc-7-583-2013

Favier, V., Krinner, G., Amory, C., Gallée, H., Beaumet, J., & Agosta, C. (2017). Antarctica-regional climate and surface mass budget. *Current Climate Change Reports*, *3*, 303–315. https://doi.org/10.1007/s40641-017-0072-z

Feser, F., Rockel, B., von Storch, H., Winterfeldt, J., & Zahn, M. (2011). Regional climate models add value to global model data: A review and selected examples. *Bulletin of the American Meteorological Society*, *92*, 1181–1192. https://doi.org/10.1175/2011BAMS3061.1

Gallée, H., Agosta, C., Gential, L., Favier, V., & Krinner, G. (2011). A downscaling approach toward high-resolution surface mass balance over Antarctica. *Surveys in Geophysics*, *32*, 507–518. https://doi.org/10.1007/s10712-011-9125-3

Gallée, H., & Gorodetskaya, I. V. (2010). Validation of a limited area model over Dome C, Antarctic Plateau, during winter. *Climate Dynamics*, *34*, 61–72. https://doi.org/10.1007/s00382-008-0499-y

Gallée, H., & Schayes, G. (1994). Development of a three-dimensional meso-y primitive equation model: Katabatic winds simulation in the area of Terra Nova Bay, Antarctica. *Monthly Weather Review*, *122*, 671–685. https://doi.org/10.1175/1520-0493(1994)122<0671:DOATDM>2.0.CO;2

Gallée, H., Trouvilliez, A., Agosta, C., Genthon, C., Favier, V., & Naaim-Bouvet, F. (2013). Transport of snow by the wind: A comparison between observations in Adélie Land, Antarctica, and simulations made with the regional climate model MAR. *Boundary-Layer Meteorology*, *146*, 133–147. https://doi.org/10.1007/s10546-012-9764-z

Genthon, C., Six, D., Gallée, H., Grigioni, P., & Pellegrini, A. (2013). Two years of atmospheric boundary layer observations on a 45-m tower at Dome C on the Antarctic plateau. *Journal of Geophysical Research: Atmospheres*, *118*, 3218–3232. https://doi.org/10.1002/jgrd.50128

Genthon, C., Town, M. S., Six, D., Favier, V., Argentini, S., & Pellegrini, A. (2010). Meteorological atmospheric boundary layer measurements and ECMWF analyses during summer at Dome C, Antarctica. *Journal of Geophysical Research*, *115*, D05104. https://doi.org/10.1029/2009JD012741

Gierens, K. (2003). On the transition between heterogeneous and homogeneous freezing. *Atmospheric Chemistry and Physics*, *3*, 437–446. https://doi.org/10.5194/acpd-2-2343-2002

Giorgi, F., & Gutowski, W. J. (2015). Regional dynamical downscaling and the CORDEX initiative. *Annual Review of Environment and Resources*, *40*, 467–490. https://doi.org/10.1146/annurev-environ-102014-021217

Giorgi, F., & Gutowski, W. J. (2016). Coordinated experiments for projections of regional climate change. *Current Climate Change Reports*, *2*, 202–210. https://doi.org/10.1007/s40641-016-0046-6

Giorgi, F., Jones, C., & Asrar, G. R. G. (2009). Addressing climate information needs at the regional level: The CORDEX framework. *WMO Bulletin*, *58*(3), 175–183.

Gorodetskaya, I. V., Kneifel, S., Maahn, M., Van Tricht, K., Thiery, W., Schween, J. H., et al. (2015). Cloud and precipitation properties from ground-based remote sensing instruments in East Antarctica. *The Cryosphere*, *9*, 285–304. https://doi.org/10.5194/tcd-8-4195-2014

Gorodetskaya, I. V., Tsukernik, M., Claes, K., Ralph, M., Neff, W., & van Lipzig, N. P. M. (2014). The role of atmospheric rivers in anomalous snow accumulation in East Antarctica. *Geophysical Research Letters*, *16*, 6199–6206. https://doi.org/10.1002/2014GL060881

Gorodetskaya, I. V., van Lipzig, N. P. M., van den Broeke, M. R., Mangold, A., Boot, W., & Reijmer, C. H. (2013). Meteorological regimes and accumulation patterns at Utsteinen, Dronning Maud Land, East Antarctica: Analysis of two contrasting years. *Journal of Geophysical Research: Atmospheres*, *118*, 1700–1715. https://doi.org/10.1002/jgrd.50177

Groh, A., & Horwath, M. (2016). The method of tailored sensitivity kernels for GRACE mass change estimates. *Geophysical Research Abstracts*, *18*(12), 065.

Gutjahr, O., Heinemann, G., Preußer, A., Willmes, S., & Drúe, C. (2016). Quantification of ice production in Laptev Sea polynyas and its sensitivity to thin-ice parameterizations in a regional climate model. *The Cryosphere*, *10*, 2999–3019. https://doi.org/10.5194/tc-10-2999-2016

Gutowski, J. W., Giorgi, F., Timbal, B., Frigon, A., Jacob, D., Kang, H. S., et al. (2016). WCRP COordinated Regional Downscaling EXperiment (CORDEX): A diagnostic MIP for CMIP6. *Geoscientific Model Development*, *9*, 4087–4095. https://doi.org/10.5194/gmd-9-4087-2016

Haid, V., Timmermann, R., Ebner, L., & Heinemann, G. (2014). Atmospheric forcing of coastal polynyas in the south-western Weddell Sea. *Antarctic Science*, *27*(4), 388–402. https://doi.org/10.1017/S0954102014000893

Handorf, D., Foken, T., & Kottmeier, C. (1999). The stable atmospheric boundary layer over an Antarctic Ice Sheet. *Boundary-Layer Meteorology*, *91*, 165–189.

Hebbinghaus, H., & Heinemann, G. (2006). LM simulations of the Greenland boundary layer, comparison with local measurements and SNOWPACK simulations of drifting snow. *Cold Regions Science and Technology*, *46*, 36–51. https://doi.org/10.1016/j.coldregions.2006.05.003

Herenz, P., Wex, H., Mangold, A., Laffineur, Q., Fleming, Z. L., Panagi, M., & Stratmann, F. (2019). CCN measurements at the Princess Elisabeth Antarctica Research Station during three austral summers. *Atmospheric Chemistry and Physics*, *19*, 275–294.

Hudson, S. R., & Brandt, R. E. (2005). A look at the surface-based temperature inversion on the Antarctic Plateau. *Journal of Climate*, *18*, 1673–1696. https://doi.org/10.1175/JCLI3360.1

Jones, J. M., Gille, S. T., Goosse, H., Abram, N. J., Canziani, P. O., Charman, D. J., et al. (2016). Assessing recent trends in high-latitude Southern Hemisphere surface climate. *Nature Climate Change*, *6*, 917–926. https://doi.org/10.1038/nclimate3103

Khain, A., Pokrovsky, A., Pinsky, M., Seifert, A., & Phillips, V. (2004). Simulation of effects of atmospheric aerosols on deep turbulent convective clouds using a spectral microphysics mixed-phase cumulus cloud model. Part I: Model description and possible applications. *Journal of Atmospheric Sciences*, *61*, 2963–2982. https://doi.org/10.1175/JAS-3350.1

King, J. C., Argentini, S. A., & Anderson, P. S. (2006). Contrasts between the summertime surface energy balance and boundary layer structure at Dome C and Halley stations, Antarctica. *Journal of Geophysical Research*, *111*, D02105. https://doi.org/10.1029/2005JD006130

King, J. C., Connolley, W. M., & Derbyshire, S. H. (2001). Sensitivity of modelled Antarctic climate to surface and boundary-layer flux parametrizations. *Quarterly Journal of the Royal Meteorological Society*, *127*, 779–794. https://doi.org/10.1002/qj.49712757304

Koenigk, T., Berg, P., & Döscher, R. (2015). Arctic climate change in an ensemble of regional CORDEX simulations. *Polar Research*, *34*(24), 603. https://doi.org/10.3402/polar.v34.24603

Köhler, C. G., & Seifert, A. (2015). Identifying sensitivities for cirrus modelling using a two-moment two-mode bulk microphysics scheme. *Tellus B: Chemical and Physical Meteorology*, *67*(24), 494. https://doi.org/10.3402/tellusb.v67.24494

König-Langlo, G., King, J. C., & Pettré, P. (1998). Climatology of the three coastal Antarctic stations Dumont d'Urville, Neumayer, and Halley. *Journal of Geophysical Research*, *103*, 10,935–10,946. https://doi.org/10.1029/97JD00527

Kuipers Munneke, P., van den Broeke, M. R., Lenaerts, J. T. M., Flanner, M. G., Gardner, A. S., & van de Berg, W. J. (2011). A new albedo parameterization for use in climate models over the Antarctic Ice Sheet. *Journal of Geophysical Research*, *116*, D05114. https://doi.org/10.1029/2010JD015113

Kyrö, E.-M., Kerminen, V.-M., Virkkula, A., Dal Maso, M., Parshintsev, J., Ruíz-Jimenez, J., et al. (2013). Antarctic new particle formation from continental biogenic precursors. *Atmospheric Chemistry and Physics*, *13*, 3527–3546. https://doi.org/10.5194/acp-13-3527-2013

Lenaerts, J. T. M., van Meijgaard, E., van den Broeke, M. R., Ligtenberg, S. R. M., Horwath, M., & Isaksson, E. (2013). Recent snowfall anomalies in Dronning Maud Land, East Antarctica, in a historical and future climate perspective. *Geophysical Research Letters*, *40*, 2684–2688. https://doi.org/10.1002/grl.50559

Lenaerts, J. T. M., Van Tricht, K., Lhermitte, S., & L'Ecuyer, T. S. (2017). Polar clouds and radiation in satellite observations, reanalyses, and climate models. *Geophysical Research Letters*, *44*, 3355–3364. https://doi.org/10.1002/2016GL072242

Lenaerts, J. T. M., & van den Broeke, M. R. (2012). Modeling drifting snow in Antarctica with a regional climate model: 1. Methods and model evaluation. *Journal of Geophysical Research*, *117*, D05108. https://doi.org/10.1029/2010JD016145

Lenaerts, J. T. M., van den Broeke, M. R., van de Berg, W. J., van Meijgaard, E., & Kuipers Munneke, P. (2012). A new, high-resolution surface mass balance map of Antarctica (1979–2010) based on regional atmospheric climate modeling. *Geophysical Research Letters*, *39*, L04501. https://doi.org/10.1029/2011GL050713

Lenaerts, J. T. M., Vizcaino, M., Fyke, J., van Kampenhout, L., & van den Broeke, M. R. (2016). Present-day and future Antarctic Ice Sheet climate and surface mass balance in the Community Earth System Model. *Climate Dynamics*, *47*, 1367–1381. https://doi.org/10.1007/s00382-015-2907-4

Ligtenberg, S. R. M., van de Berg, W. J., van den Broeke, M. R., Rae, J. G. L., & van Meijgaard, E. (2013). Future surface mass balance of the Antarctic Ice Sheet and its influence on sea level change, simulated by a regional atmospheric climate model. *Climate Dynamics*, *41*, 867–884. https://doi.org/10.1007/s00382-013-1749-1

Liston, G. E., Haehnel, R. B., Sturm, M., Hiemstra, C. A., Berezovskaya, S., & Tabler, R. D. (2007). Simulating complex snow distributions in windy environments using SnowTran-3D. *Journal of Glaciology*, *53*(181), 241–256. https://doi.org/10.3189/172756507782202865

Liu, H., Jezek, K. C., Li, B., & Zhao, Z. (2015). Radarsat Antarctic Mapping Project Digital Elevation Model. Version 2. https://doi.org/10.5067/8JKNEW6BFRVD

Martin-Español, A., Bamber, J. L., & Zammit-Mangion, A. (2017). Constraining the mass balance of East Antarctica. *Geophysical Research Letters*, *44*, 4168–4175. https://doi.org/10.1002/2017GL072937

Medley, B., & Thomas, E. R. (2019). Increased snowfall over the Antarctic Ice Sheet mitigated twentieth-century sea-level rise. *Nature Climate Change*, *9*, 34–39. https://doi.org/10.1038/s41558-018-0356-x

Monaghan, A. J., Bromwich, D. H., Fogt, R. L., Wang, S.-H., Mayewski, P. A., Dixon, D. A., et al. (2006). Insignificant change in Antarctic snowfall since the International Geophysical Year. *Science*, *313*, 827–831. https://doi.org/10.1126/science.1128243

Moradi, I., Soden, B., Ferraro, R., Arkin, P., & Vömel, H. (2013). Assessing the quality of humidity measurements from global operational radiosonde sensors. *Journal of Geophysical Research: Atmospheres*, *118*, 8040–8053. https://doi.org/10.1002/jgrd.50589

Nishimura, K., Yokoyama, C., Ito, Y., Nemoto, M., Naaim-Bouvet, F., Bellot, H., & Fujita, K. (2014). Snow particle speeds in drifting snow. *Journal of Geophysical Research: Atmospheres*, *119*, 9901–9913. https://doi.org/10.1002/2014JD021686

Oleson, K. W., & Lawrence, D. M. (2013). Technical description of version 4.5 of the Community Land Model (CLM) (Tech. Rep. July). Boulder, Colorado: NCAR. https://doi.org/10.5065/D6RR1W7M

Parish, T. R., & Bromwich, D. H. (1986). The inversion wind pattern over West Antarctica. *Monthly Weather Review*, *114*, 849–860. https://doi.org/10.1175/1520-0493(1986)114<0849:TIWPOW>2.0.CO;2

Parish, T. R., & Bromwich, D. H. (1987). The surface windfield over the Antarctic ice sheets. *Nature*, *328*, 51–54. https://doi.org/10.1038/328051a0

Parish, T. R., & Bromwich, D. H. (2007). Reexamination of the near-surface airflow over the Antarctic continent and implications on atmospheric circulations at high southern latitudes. *Monthly Weather Review*, *135*, 1961–1973. https://doi.org/10.1175/MWR3374.1

Parish, T. R., & Cassano, J. J. (2003). The role of katabatic winds on the Antarctic surface wind regime. *Monthly Weather Review*, *131*, 317–333. https://doi.org/10.1175/1520-0493(2003)131<0317:TROKWO>2.0.CO;2

Paukert, M., & Hoose, C. (2014). Modeling immersion freezing with aerosol-dependent prognostic ice nuclei in Arctic mixed-phase clouds. *Journal of Geophysical Research: Atmospheres*, *119*, 9073–9092. https://doi.org/10.1002/2014JD021917

Phillips, V. T. J., DeMott, P. J., & Andronache, C. (2008). An empirical parameterization of heterogeneous ice nucleation for multiple chemical species of aerosol. *Journal of the Atmospheric Sciences*, *65*, 2757–2783. https://doi.org/10.1175/2007JAS2546.1

Pietroni, I., Argentini, S., & Petenko, I. (2014). One year of surface-based temperature inversions at Dome C, Antarctica. *Boundary-Layer Meteorology*, *150*, 131–151. https://doi.org/10.1007/s10546-013-9861-7

Reijmer, C. H., van Meijgaard, E., & van den Broeke, M. R. (2005). Evaluation of temperature and wind over Antarctica in a regional atmospheric climate model using 1 year of automatic weather station data and upper air observations. *Journal of Geophysical Research*, *110*, D04103. https://doi.org/10.1029/2004JD005234

Rignot, E., Velicogna, I., van den Broeke, M. R., Monaghan, A., & Lenaerts, J. T. M. (2011). Acceleration of the contribution of the Greenland and Antarctic ice sheets to sea level rise. *Geophysical Research Letters*, *38*, L05503. https://doi.org/10.1029/2008GM000741/summary

Rockel, B., Will, A., & Hense, A. (2008). The regional climate model COSMO-CLM (CCLM). *Meteorologische Zeitschrift*, *17*(4), 347–348. https://doi.org/10.1127/0941-2948/2008/0309

Rowe, P. M., Miloshevich, L. M., Turner, D. D., & Walden, V. P. (2008). Dry bias in Vaisala RS90 radiosonde humidity profiles over Antarctica. *Journal of Atmospheric and Oceanic Technology*, *25*, 1529–1541. https://doi.org/10.1175/2008JTECHA1009.1

Rummukainen, M. (2016). Added value in regional climate modeling. *Wiley Interdisciplinary Reviews: Climate Change*, *7*, 145–159. https://doi.org/10.1002/wcc.378

Sanz Rodrigo, J. (2011). On Antarctic wind engineering (PhD thesis). Université Libre de Bruxelles.

Sanz Rodrigo, J., Buchlin, J. M., van Beeck, J., Lenaerts, J. T. M., & van den Broeke, M. R. (2013). Evaluation of the antarctic surface wind climate from ERA reanalyses and RACMO2/ANT simulations based on automatic weather stations. *Climate Dynamics*, *40*, 353–376. https://doi.org/10.1007/s00382-012-1396-y

Schaaf, C. B., Gao, F., Strahler, A. H., Lucht, W., Li, X., Tsang, T., et al. (2002). First operational BRDF, albedo nadir reflectance products from MODIS. *Remote Sensing of Environment*, *83*, 135–148. https://doi.org/10.1016/S0034-4257(02)00091-3

Schlosser, E., Manning, K. W., Powers, J. G., Duda, M. G., Birnbaum, G., & Fujita, K. (2010). Characteristics of high-precipitation events in Dronning Maud Land, Antarctica. *Journal of Geophysical Research*, *115*, D14107. https://doi.org/10.1029/2009JD013410

Schmidt, R. A. (1982). Properties of blowing snow. *Reviews of Geophysics and Space Physics*, *20*(1), 39–44. https://doi.org/10.1029/RG020i001p00039

Scinocca, J. F., Kharin, V. V., Jiao, Y., Qian, M. W., Lazare, M., Solheim, L., et al. (2016). Coordinated global and regional climate modeling. *Journal of Climate*, *29*, 17–35. https://doi.org/10.1175/JCLI-D-15-0161.1

Seifert, A., & Beheng, K. D. (2006). A two-moment cloud microphysics parameterization for mixed-phase clouds. Part 1: Model description. *Meteorology and Atmospheric Physics*, *92*, 45–66. https://doi.org/10.1007/s00703-005-0112-4

Shepherd, A., Ivins, E. R., Geruo, A., Barletta, V. R., Bentley, M. J., Bettadpur, S., et al. (2012). A reconciled estimate of ice-sheet mass balance. *Science*, *338*, 1183–1189.

Smeets, C. J. P. P., & van den Broeke, M. R. (2008). Temporal and spatial variations of the aerodynamic roughness length in the ablation zone of the Greenland Ice Sheet. *Boundary-Layer Meteorology*, *128*, 315–338. https://doi.org/10.1007/s10546-008-9291-0

Souverijns, N., Gossart, A., Gorodetskaya, I. V., Lhermitte, S., Mangold, A., Laffineur, Q., et al. (2018). How does the ice sheet surface mass balance relate to snowfall? Insights from a ground-based precipitation radar in East Antarctica. *The Cryosphere*, *12*(6), 1987–2003. https://doi.org/10.5194/tc-12-1987-2018

Souverijns, N., Gossart, A., Lhermitte, S., Gorodetskaya, I. V., Kneifel, S., Maahn, M., et al. (2017). Estimating radar reflectivity—Snowfall rate relationships and their uncertainties over Antarctica by combining disdrometer and radar observations. *Atmospheric Research*, *196*, 211–223. https://doi.org/10.1016/j.atmosres.2017.06.001

Stocker, T., Qin, D., Plattner, G.-K., Alexander, L., Allen, S., Bindoff, N., et al. (2013). Technical summary. In T. Stocker, et al. (Eds.), *Climate change 2013: The physical science basis. Contribution of Working Group I to the Fifth Assessment Report of the Intergovernmental Panel on Climate Change* (pp. 33–115). Cambridge, United Kingdom and New York, NY: Cambridge University Press.

Stroeve, J., Box, J. E., Gao, F., Liang, S., Nolin, A., & Schaaf, C. (2005). Accuracy assessment of the MODIS 16-day albedo product for snow: Comparisons with Greenland in situ measurements. *Remote Sensing of Environment*, *94*, 46–60. https://doi.org/10.1016/j.rse.2004.09.001

Takahashi, S. (1988). A preliminary estimation of drifting snow convergence alond a flow line of Shirase Glacier, East Antarctica. *Bulletin of Glacier Research*, *6*, 41–46.

Tapley, B. D., Bettadpur, S., Ries, J. C., Thompson, P. F., & Watkins, M. M. (2004). GRACE measurements of mass variability in the Earth system. *Science*, *305*, 503–505. https://doi.org/10.1126/science.1099192

Thiery, W., Gorodetskaya, I. V., Bintanja, R., van Lipzig, N. P. M., van den Broeke, M. R., Reijmer, C. H., & Kuipers Munneke, P. (2012). Surface and snowdrift sublimation at Princess Elisabeth station, East Antarctica. *The Cryosphere*, *6*, 841–857. https://doi.org/10.5194/tc-6-841-2012

Thomas, E. R., Van Wessem, J. M., Roberts, J., Isaksson, E., Schlosser, E., Fudge, T. J., et al. (2017). Regional Antarctic snow accumulation over the past 1000 years. *Climate of the Past*, *13*, 1491–1513. https://doi.org/10.5194/cp-13-1491-2017

Turner, J., Colwell, S. R., Marshall, G. J., Lachlan-Cope, T. A., Carleton, A. M., Jones, P. D., et al. (2004). The SCAR READER project: Toward a high-quality database of mean Antarctic meteorological observations. *Journal of Climate*, *17*, 2890–2898. https://doi.org/10.1175/1520-0442(2004)017<2890:TSRPTA>2.0.CO;2

van As, D., van den Broeke, M. R., & Helsen, M. M. (2006). Structure and dynamics of the summertime atmospheric boundary layer over the Antarctic Plateau: 1. Measurements and model validation. *Journal of Geophysical Research*, *111*, D07102. https://doi.org/10.1029/2005JD005948

van Kampenhout, L., Lenaerts, J. T. M., Lipscomb, W. H., Sacks, W. J., Lawrence, D. M., Slater, A. G., & van den Broeke, M. R. (2017). Improving the representation of polar snow and firn in the Community Earth System Model. *Journal of Advances in Modeling Earth Systems*, *9*, 2583–2600. https://doi.org/10.1002/2017MS000988

van Lipzig, N. P. M., King, J. C., Lachlan-Cope, T. A., & van den Broeke, M. R. (2004). Precipitation, sublimation, and snow drift in the Antarctic Peninsula region from a regional atmospheric model. *Journal of Geophysical Research*, *109*, D24106. https://doi.org/10.1029/2004JD004701

van Lipzig, N. P. M., Marshall, G. J., Orr, A., & King, J. C. (2008). The relationship between the Southern Hemisphere annular mode and Antarctic Peninsula summer temperatures: Analysis of a high-resolution model climatology. *Journal of Climate*, *21*, 1649–1668. https://doi.org/10.1175/2007JCLI1695.1

van Lipzig, N. P. M., Turner, J., Colwell, S. R., & van den Broeke, M. R. (2004). The near-surface wind field over the Antarctic continent. *International Journal of Climatology*, *24*(15), 1973–1982. https://doi.org/10.1002/joc.1090

van Lipzig, N. P. M., van Meijgaard, E., & Oerlemans, J. (1999). Evaluation of a regional atmospheric model using measurements of surface heat exchange processes from a site in Antarctica. *Monthly Weather Review*, *127*, 1994–2011.

van Lipzig, N. P. M., van Meijgaard, E., & Oerlemans, J. (2002). The spatial and temporal variability of the surface mass balance in Antarctica: Results from a regional atmospheric climate model. *International Journal of Climatology*, *22*(10), 1197–1217. https://doi.org/10.1002/joc.798

Van Tricht, K., Gorodetskaya, I. V., Lhermitte, S., Turner, D. D., Schween, J. H., & Van Lipzig, N. P. M. (2014). An improved algorithm for polar cloud-base detection by ceilometer over the ice sheets. *Atmospheric Measurement Techniques*, *7*(5), 1153–1167. https://doi.org/10.5194/amt-7-1153-2014

Van Tricht, K., Lhermitte, S., Lenaerts, J. T. M., Gorodetskaya, I. V., L'Ecuyer, T. S., Noël, B., et al. (2016). Clouds enhance Greenland ice sheet meltwater runoff. *Nature Communications*, *7*(10), 266. https://doi.org/10.1038/ncomms10266

van Wessem, J. M., Reijmer, C. H., Lenaerts, J. T. M., van De Berg, W. J., van Den Broeke, M. R., & van Meijgaard, E. (2014). Updated cloud physics in a regional atmospheric climate model improves the modelled surface energy balance of Antarctica. *The Cryosphere*, *8*, 125–135. https://doi.org/10.5194/tc-8-125-2014

van Wessem, J. M., Reijmer, C. H., Morlighem, M., Mouginot, J., Rignot, E., Medley, B., et al. (2014). Improved representation of East Antarctic surface mass balance in a regional atmospheric climate model. *Journal of Glaciology*, *60*(222), 761–770. https://doi.org/10.3189/2014JoG14J051

van Wessem, J. M., Reijmer, C. H., van de Berg, W. J., van den Broeke, M. R., Cook, A. J., van Ulft, L. H., & van Meijgaard, E. (2015). Temperature and wind climate of the Antarctic Peninsula as simulated by a high-resolution Regional Atmospheric Climate Model. *Journal of Climate*, *28*, 7306–7326. https://doi.org/10.1175/JCLI-D-15-0060.1

van Wessem, J. M., van de Berg, W. J., Noël, B. P. Y., van Meijgaard, E., Amory, C., Birnbaum, G., et al. (2018). Modelling the climate and surface mass balance of polar ice sheets using RACMO2—Part 2: Antarctica (1979–2016). *The Cryosphere*, *12*, 1479–1498. https://doi.org/10.5194/tc-12-1479-2018

van de Berg, W. J., & Medley, B. (2016). Brief communication: Upper-air relaxation in RACMO2 significantly improves modelled interannual surface mass balance variability in Antarctica. *The Cryosphere*, *10*, 459–463. https://doi.org/10.5194/tc-10-459-2016

van de Berg, W., van den Broeke, M., Reijmer, C., & van Meijgaard, E. (2005). Characteristics of the Antarctic surface mass balance, 1958–2002, using a regional atmospheric climate model. *Annals of Glaciology*, *41*(1), 97–104. https://doi.org/10.3189/172756405781813302

van den Broeke, M., Bamber, J., Ettema, J., Rignot, E., Schrama, E., van de Berg, W. J., et al. (2009). Partitioning recent Greenland mass loss. *Science*, *326*, 984–986. https://doi.org/10.1126/science.1178176

van den Broeke, M. R., Reijmer, C. H., & Van de Wal, R. S. W. (2004). A study of the surface mass balance in Dronning Maud Land, Antarctica, using automatic weather stations. *Journal of Glaciology*, *50*(171), 565–582. https://doi.org/10.3189/172756504781829756

van den Broeke, M. R., & van Lipzig, N. P. M. (2003). Factors controlling the near-surface wind field in Antarctica. *Monthly Weather Review*, *131*, 733–743. https://doi.org/10.1175/1520-0493(2003)131<0733:FCTNSW>2.0.CO;2

van den Broeke, M. R., & van Lipzig, N. P. M. (2004). Changes in Antarctic temperature, wind and precipitation in response to the Antarctic Oscillation. *Annals of Glaciology*, *39*, 119–126. https://doi.org/10.3189/172756404781814654

Vionnet, V., Brun, E., Morin, S., Boone, A., Faroux, S., Le Moigne, P., et al. (2012). The detailed snowpack scheme Crocus and its implementation in SURFEX v7.2. *Geoscientific Model Development*, *5*, 773–791. https://doi.org/10.5194/gmd-5-773-2012

Wacker, U., Ries, H., & Schättler, U. (2009). Precipitation simulation for Dronning Maud Land using the COSMO Model. *Antarctic Science*, *21*(6), 643–662. https://doi.org/10.1017/S0954102009990149

Walden, V. P., Warren, S. G., & Tuttle, E. (2003). Atmospheric ice crystals over the Antarctic Plateau in winter. *Journal of Applied Meteorology*, *42*(10), 1391–1405. https://doi.org/10.1175/1520-0450(2003)042<1391:AICOTA>2.0.CO;2

Wang, Y., Ding, M., van Wessem, J. M., Schlosser, E., Altnau, S., van den Broeke, M. R., et al. (2016). A comparison of Antarctic Ice Sheet surface mass balance from atmospheric climate models and in situ observations. *Journal of Climate*, *29*, 5317–5337. https://doi.org/10.1175/JCLI-D-15-0642.1

Will, A., Akhtar, N., Brauch, J., Breil, M., Davin, E., Ho-Hagemann, H. T., et al. (2017). The COSMO-CLM 4.8 regional climate model coupled to regional ocean, land surface and global earth system models using OASIS3-MCT: Description and performance. *Geoscientific Model Development*, *10*, 1549–1586. https://doi.org/10.5194/gmd-10-1549-2017

Wouters, H., Demuzere, M., Blahak, U., Fortuniak, K., Maiheu, B., Camps, J., et al. (2016). The efficient urban canopy dependency parametrization (SURY) v1.0 for atmospheric modelling: Description and application with the COSMO-CLM model for a Belgian summer. *Geoscientific Model Development*, *9*, 3027–3054. https://doi.org/10.5194/gmd-9-3027-2016

Xin, Y., Bian, L., Rinke, A., & Dethloff, K. (2014). Simulation and evaluation of 2-m temperature over Antarctica in polar regional climate model. *Science China Earth Sciences*, *57*(4), 703–709. https://doi.org/10.1007/s11430-013-4709-z

Zhou, X., Matthes, H., Rinke, A., Klehmet, K., Heim, B., Dorn, W., et al. (2014). Evaluation of Arctic land snow cover characteristics, surface albedo, and temperature during the transition seasons from regional climate model simulations and satellite data. *Advances in Meteorology*, *2014*(604), 157. https://doi.org/10.1155/2014/604157

Zwally, H. J., Giovinetto, M. B., Beckley, M. A., & Saba, J. L. (2012). Antarctic and Greenland drainage systems.